https://doi.org/10.5194/egusphere-2026-2728
Preprint. Discussion started: 4 August 2026

Climate Models Underestimate Pre-Industrial Fire Emissions

Noah Liguori-Bills[1], Catherine E. Scott[2], Ken S. Carslaw[2], Natalie Kehrwald[3], Stijn Hantson[4], Susan Kaspari[5], Carlo Barbante[6], Elena Barbaro[6], Paolo Gabrielli[7,#], Roberta Zangrando[6], Lonnie G Thompson[8,9], and Douglas S. Hamilton[1]

[1]Marine, Earth, and Atmospheric Sciences, North Carolina State University, Raleigh, NC, USA.
[2]School of Earth, Environment and Sustainability, University of Leeds, Leeds, United Kingdom.
[3]US Geological Survey, Geosciences and Environmental Change Science Center, Denver, CO, USA.
[4]School of Sciences and Engineering, Universidad del Rosario, Bogotá, Colombia.
[5]Department of Geological Sciences, Central Washington University, Ellensburg, WA, USA.
[6]Ca'Foscari University of Venice, Mestre, Veneto, Italy
[7] Italian Glaciological Committee c/o University of Turin, Turin, Italy
[8]Byrd Polar and Climate Research Center, The Ohio State University, Columbus, OH, USA.
[9]School of Earth Sciences, The Ohio State University, Columbus, OH, USA.
[#]Now at the Metropolitan Water District of Southern California, 700 Moreno Ave, La Verne, CA, 91750, USA

Corresponding author: **Douglas S. Hamilton (dshamil3@ncsu.edu)**

Key Points:

- Ice cores and climate models disagree on changes in black carbon from 1850 to 1980
- CMIP likely underestimated the magnitude of preindustrial fire emissions in many regions
- Changes in aerosol transport and processes are a secondary consideration after initial emissions

https://doi.org/10.5194/egusphere-2026-2728
Preprint. Discussion started: 4 August 2026

Abstract

An improved understanding of how fire regimes changed from the pre-industrial to the present-day is required to reduce uncertainty in anthropogenic aerosol radiative forcing. Direct observations of pre-industrial fires are scarce so here we evaluate assumptions about historical fire regime change using black carbon data from polar and alpine ice core records and global climate model simulations from the Coupled Model Intercomparison Project Phase 6 (CMIP6) and the Large Ensemble Community Project (LENS). Black carbon is a tracer of both natural and anthropogenic combustion, enabling comparison of fire and industrial combustion emission changes from the pre-industrial (1850 CE) to the present day (1980 CE). Polar ice core records indicate relatively modest increases in mean and median 1980 CE/1850 CE black carbon ratios of 1.27 and 1.15, compared with 2.89 and 2.64 in the CMIP6 ensemble, respectively. Alpine ice cores record larger increases (mean 2.31; median 1.93), compared with even larger increases simulated in CMIP6 in alpine regions (mean 3.59; median 2.50). We tested three possibilities to explain the difference between black carbon simulated by models and recorded in observations: (1) pre-industrial fire emissions are too low in models; (2) changes in aerosol transport over the Industrial Era using data from LENS; and (3) differences in modelled aerosol properties and deposition parameterizations using CESM2 data. Analysis of these different drivers revealed that the most effective method to reconcile the model-observation disparity is to increase pre-industrial fire emissions in the models and that transport or aerosol properties are of secondary consideration.

Plain Language Summary

Ice cores preserve changes in landscape fires and human-caused combustion. In this study, we compared ice core data from every continent, except Oceania, to computer model simulations of fire. We found a large disagreement in the 1850 CE to 1980 CE black carbon ratio. After exploring changes in emissions, transport, and aerosol microphysical processes as potential reasons for this disagreement, our results suggested that fire emission input datasets for climate models are the primary cause.

https://doi.org/10.5194/egusphere-2026-2728
Preprint. Discussion started: 4 August 2026

1 Introduction

Earth System models (ESM) are powerful tools used to construct the history and future of Earth's climate through the simulation of key land-atmosphere-ocean processes, including the influence of landscape fire and other open burning practices on climate, radiative forcing, and atmospheric composition. To do so, ESMs can either use an interactive fire model embedded within a land-vegetation model framework or use prescribed gas and aerosol emission datasets that represent how fire regimes change over a time period of interest. For climate studies, it is important to understand how fire (defined here as the sum of all natural landscape and anthropogenic open burning fires) shapes both the pre-industrial (PI) atmospheric state and how changes in fire alter the atmospheric burden of aerosol and gases over the Industrial Era to the present day (PD) (Carslaw et al., 2013; Hamilton et al., 2018). The Sixth Coupled Model Inter-Comparison Project (CMIP6) experiment is an ensemble of ESMs that produced historical simulated climate relevant data. The experiment defines 1850 CE as 'pre-industrial', corresponding to the start of large-scale industrialization (Eyring et al., 2016).

A wide variety of processes can change the energy balance of the atmosphere over time, including human driven perturbations such as changing greenhouse gas concentrations or aerosol emission rates. Quantification of human activity's influence on the atmospheric energy balance is termed 'anthropogenic radiative forcing.' However, assessment of this forcing often excludes changes to natural aerosol and gas emission sources, including information about fire regimes (Mahowald et al., 2024). Including a representation of changes in fire over the historical period is critical for calculating aerosol radiative forcing. Fire helps establish both a PI atmospheric composition baseline and is a key component of calculating the PI to PD aerosol radiative forcing (Carslaw et al., 2017; Hamilton et al., 2018; Simpkins, 2018; Wan et al., 2021).

Fires emit a multitude of gases and aerosols during combustion (Andrea 2017). Fire aerosols can either absorb or scatter solar radiation in the atmosphere, leading to heating or cooling effects (Rap et al., 2013; Collins et al., 2017). Fire aerosols also function as cloud condensation nuclei (CCN), affecting the atmospheric energy balance by changing cloud drop concentrations and by initiating a series of cloud adjustments that affect cloud albedo (Ackerman et al., 2000; Andreae & Rosenfeld, 2008; Cozic et al., 2007, 2008; Koch & Del Genio, 2010). Furthermore, certain fire aerosols such as black carbon (BC) can also change Earth's energy balance when deposited on snow and ice by decreasing surface albedo, and thus, increasing snow and glacial melt rates by absorbing more solar radiation compared to pure ice or snow (Gabbi et al., 2015; Hadley & Kirchstetter, 2012; Hansen & Nazarenko, 2004; Jacobson, 2004; Lee et al., 2013; Skiles et al., 2018).

Due to the impacts of BC aerosol load, a product of incomplete combustion from both natural and anthropogenic sources (Bond et al. 2013), on both the atmospheric and terrestrial energy balance, it is especially important to understand how BC concentrations have changed over time. In the absence of anthropogenic industrial activity, landscape fires were the major BC aerosol emission source (Hamilton et al., 2018). Over one hundred years later, at the turn of the 21st century, fire had become a minor contributor to BC emissions in a more polluted, anthropogenic

https://doi.org/10.5194/egusphere-2026-2728
Preprint. Discussion started: 4 August 2026

emission dominated, atmosphere (e.g., Bond et al., 2007; van der Werf et al., 2017). Over this time period, changes in fire regimes were influenced by both climate and non-climate factors, including increasing population density, and human land use and land cover change (Foley et al., 2005; Jones et al., 2022; Mollicone et al., 2006; Pausas & Keeley, 2014; Rudel et al., 2009).

Drivers of fire regimes vary regionally and include changes in climate, vegetation, human population, and land use management (e.g., Aragão et al., 2018; Archibald et al., 2010; Baker & Spracklen, 2019; Cahoon et al., 1992; Giglio et al., 2018; Jones et al., 2022; Nikonovas et al., 2020; Staal et al., 2018). While precipitation and other climatic controls historically played a dominant role in regulating fire occurrence and severity, the human influence on the landscape has increasingly shaped fire regimes since the PI period (Pechony & Shindell, 2010). The relationship between human population and fire activity is generally considered non-monotonic: at low population densities, increased ignitions tend to enhance fire occurrence, whereas at higher population densities, land fragmentation, agropastoral land conversion, and active fire suppression increasingly limit fire spread (Andela et al., 2017; Archibald et al., 2012; Kelley et al., 2019; Pechony & Shindell, 2010). As a result, global burned area has declined over the late 20th and early 21st centuries (Andela et al., 2017; Ward et al., 2012). However, the complexity of these human-driven changes in fire regimes is not always fully represented in ESMs (Li et al., 2019) or the fire emission inventories used by them (Hamilton et al., 2018). Failure to capture the human-driven decline in burned area since the PI can propagate into overestimates of the radiative cooling effect of anthropogenic aerosol emissions (Hamilton et al., 2018), with implications for estimates of climate sensitivity (Mahowald et al., 2024). Improving reconstructions of historical BC and other fire-related emissions is therefore critical for reducing uncertainty in PI to PD aerosol radiative forcing (Bellouin et al., 2020; Bender, 2020).

Hamilton et al. (2018) was the first study to evaluate the use of CMIP fire emission datasets against ice core data in an attempt to quantify how uncertainty in historical fire regime change contributes to the uncertainty in PI to PD aerosol radiative forcing. The authors compared 4 Northern Hemisphere (i.e., the hemisphere in which anthropogenic aerosol radiative forcing is largest) ice core records of BC against global aerosol model simulations. Results suggested that fire emissions were likely to be between 2x to 4x higher in the PI than was estimated in the CMIP6 emission dataset. Revised modeling that included the higher fire emission reconstruction resulted in reductions of the PI to PD cloud albedo forcing between 35% and 91% compared to using CMIP6 emission data. The authors then followed this aerosol focused study by exploring the impacts of fire emissions on ozone radiative forcing, finding that the revised fire inventories decreased PI to PD ozone radiative forcing by up to 29% (Rowlinson et al., 2020). A follow-on study by Liu et al. (2021) focused on the Southern Hemisphere ice core record, including 14 Antarctic ice cores and 1 central Andean core from Illimani, Bolivia. Their results supported Hamilton et al. (2018)'s findings that PI fire emissions were likely to be higher in the PI compared to the PD and that the decline in Southern Hemisphere fire BC emissions from 1750 to 2000 CE was large enough to offset anthropogenic aerosol radiative forcing over the same period. Other recent studies include Moseid et al. (2022) who found that cores in the European Alps and

https://doi.org/10.5194/egusphere-2026-2728
Preprint. Discussion started: 4 August 2026

Greenland have a pre-1950 BC maxima, agreeing with the charcoal record, while most CMIP6 models suggest a post-1950 maxima (Moseid et al., 2022; Zhang et al., 2024). Faïn et al., (2025) discovered that the growth rate of Northern Hemisphere carbon monoxide (CO) records (another proxy of combustion) and 7 Aerosol Chemistry Model Intercomparison Project (AerChemMIP) models diverge from 1920 to 1980. Charcoal record studies have also long supported these ice record based conclusions by being the first to suggest that global burned area has decreased from the PI to the PD (e.g., Arora & Melton, 2018; Marlon et al., 2008).

Investigating the discrepancies between PI to PD BC changes in CMIP and observational ice core records is of timely importance, given CMIP7 emission datasets are in development (Durack et al., 2025). In this study we investigate, for the first time, all three potential sources of uncertainty in the disagreement between climate model-simulated and ice core-recorded changes in BC over the Industrial Era: (1) aerosol emissions; (2) aerosol mass and deposition processes; and (3) aerosol transport pathways (Table S1). To explore each of these potential sources of uncertainty, this study builds on previous work by assembling a comprehensive ice core dataset of combustion proxy data (a total of 37 ice cores; 36 of BC and 1 of levoglucosan) and then comparing the ice core data to three ESM ensembles of simulated BC: CMIP6, the Large Ensemble Community Project (LENS1; that uses CMIP5 emission data), and also the CESM2 subset of CMIP6. Finally, we tested the sensitivity of our results to the choice of definition of what year constitutes the "PI" baseline (Table S2).

2 Data and Methods

2.1 Ice Core Data

Ice core records of BC deposition provide an observational record of natural and anthropogenic combustion and are therefore useful tools for validating ESMs' modeled history of BC deposition (McConnell, 2010). Ice cores are dated with various, and often multiple, methods to minimize errors in constructing data time series. Water isotopes, trace elements, major ions and BC often exhibit seasonal variations that can be used to annually date ice cores (Andersen et al., 2006; Sigl et al., 2016). Independent age markers such as tritium concentrations, beta radioactivity, Cs^{137} and Pb^{210} and ^{14}C are used to constrain ice core depth-age scales (e.g., Pinglot et al., 2003; Fang et al., 2023). Due to the use of multiple, independent dating techniques the typical dating age uncertainty for our study period (i.e., from the mid-19th century to the late 20th century) ranges from ±0.5 to ±2 years, per dated layer (Andersen et al., 2006; Eichler et al., 2000), meaning that uncertainty does not significantly differ across the ice core depths analyzed in this study.

Data from a total of 37 ice cores (36 BC records and 1 levoglucosan record) were assembled from the literature for this study (Figure 1 and Table S3). For simplicity, we count the levoglucosan record as a "BC record" herein when discussing global averages, as levoglucosan is a biomass

https://doi.org/10.5194/egusphere-2026-2728
Preprint. Discussion started: 4 August 2026

burning marker derived from combusting cellulose in plants and therefore also traces past fire activity. Ice cores were selected for analysis if they met the following two criteria:

1. Provided a record of fire (normally BC) within the Industrial Era (defined here as post 1850 CE to follow CMIP6 protocols)
2. The difference between the most recent and oldest years was at least 100 years.

These criteria resulted in at least one ice core being identified within every continent except Oceania (Figure 1). Core 9 in Africa used levoglucosan data as an indicator of burning, instead of BC, because it is the only ice core record of fire in Africa available to the authors at this time. Due to the high variability in levoglucosan records, a LOESS smoothing with a parameter of 0.2 was used to smooth the data prior to analysis (Figure S1).

We compared the compiled BC ice core dataset with climate model BC output (Section 2.3) at the geographic locations of the ice cores. In both the ice core records and the climate model emission data and subsequent simulation outputs, total BC represents the combined contribution of fire and anthropogenic combustion sources. Accordingly, comparisons between the ice core observations and modeled BC reflect the relative evolution of these two major BC source categories: fire and anthropogenic emissions.

https://doi.org/10.5194/egusphere-2026-2728
Preprint. Discussion started: 4 August 2026

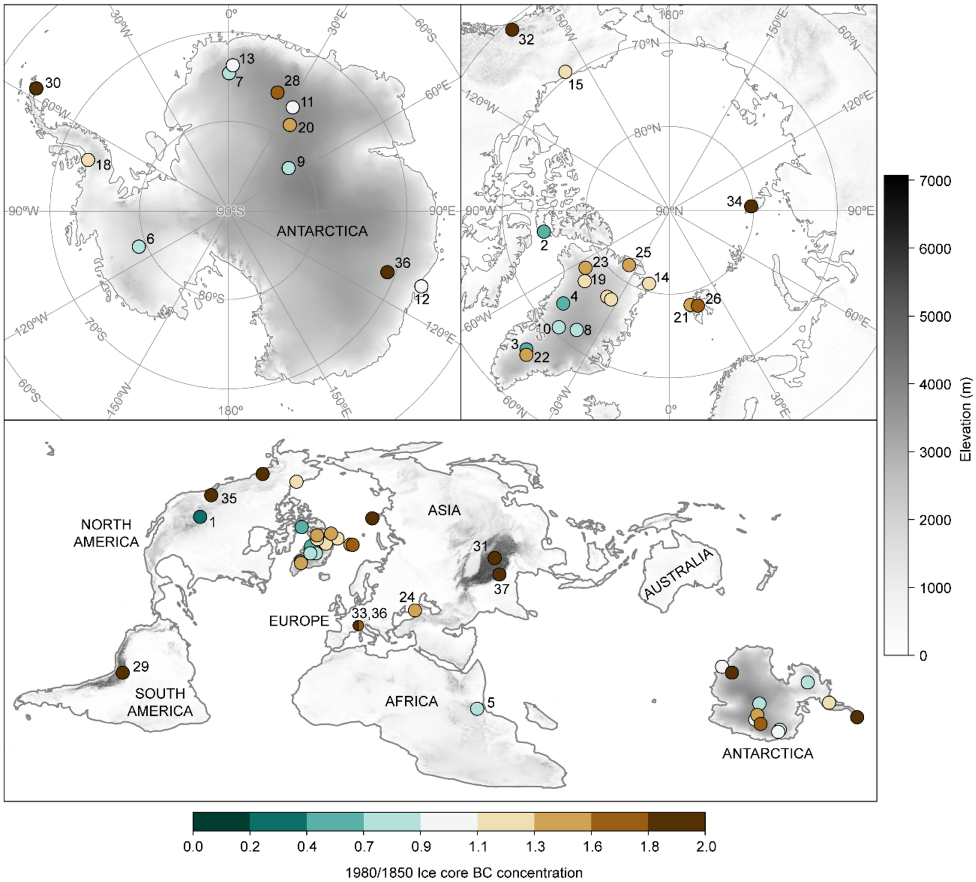

Figure 1. Location of all 37 ice core records used in this study. Ice core colors represent present day (PD; 1980 CE) / pre-industrial (PI; 1850 CE) black carbon (BC) ratios (or levoglucosan in the case of the African ice core) where blue and brown represent lower and higher BC concentration in the PD relative to the PI, respectively. A white color represents an ice core with little to no change in BC from the PI to the PD. Ice core numbers are ordered according to their PD/PI BC ratio where #1 has the lowest ratio (0.40) and #37 has the highest ratio (6.78). Elevation is shown in greyscale. Extended information on the ice cores including their exact location, dating methods, and common naming abbreviations is reported in Table S3.

2.2 Defining the Pre-Industrial (PI) and Present Day (PD)

To assess the uncertainty associated with the choice of PI baseline year, we evaluated how different PI definitions affect ice core–derived changes in BC (Section 3.5). Specifically, PI was alternatively defined as 1750 CE, 1800 CE, 1850 CE, and 1900 CE. The CMIP6 historical experiment has a start date of 1850 CE (Eyring et al., 2016). We therefore defined the PI as the

https://doi.org/10.5194/egusphere-2026-2728
Preprint. Discussion started: 4 August 2026

25-year mean after 1850 CE (inclusive) for the main results within this study because that is the earliest date with model results from CMIP6 and LENS.

The most recent values in the ice core dataset are limited by the year they were drilled and the thickness of firn that was unsuitable for analysis. In the compiled dataset ice core end date values ranged from 1950 CE to post 2010 CE. Herein, the PD was defined as the 25-year mean preceding 1980 CE (inclusive) because it represented the most recent date where nearly all (36/37) ice cores contained sample data within 5 years of 1980 (Figures S2, S3). 1980 CE also represents a scientific transition point to a new satellite data era, making assessments of post-1980 changes in atmospheric composition more robust with the advent of a global remote sensing view. Averaging windows from 5 to 30 years were considered for the PI and PD. A 25-year averaging window was ultimately chosen for analysis because it provided the lowest standard deviation across ice core data and captured fire regimes with longer (decadal scale) return intervals (Figure S4).

2.3 Defining Local, Continental, and Hemispheric Study Regions

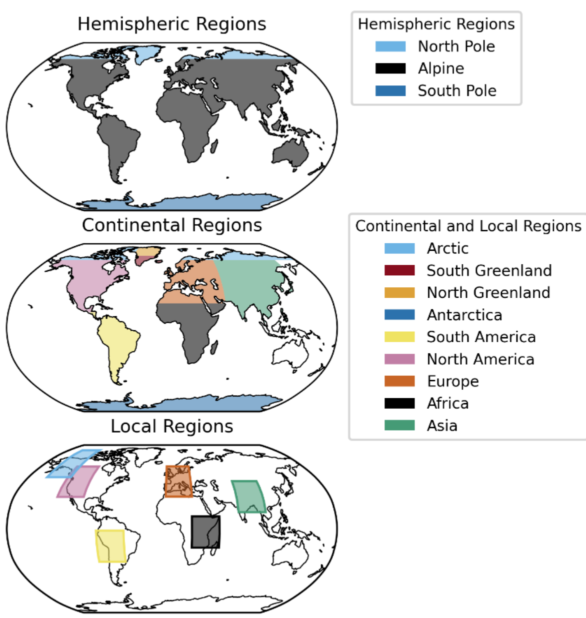

Figure 2. Definitions of each hemispheric, continental, and local emission region used in this study. Hemispheric and continental regions are color coded and defined in the legend.

https://doi.org/10.5194/egusphere-2026-2728
Preprint. Discussion started: 4 August 2026

This study defines hemispheric regions for broader spatial analysis, including the “North Pole”, “South Pole”, and “Alpine” regions corresponding to ice cores above 66.6° North latitude, within Antarctica, and all other regions combined, respectively (Figure 2 and Table S4).

Continental regions were defined according to standard continent definitions with the exception of the Arctic (Figure 2). The Arctic continental region was defined by latitudes within the Arctic circle (i.e., greater than 66.6° latitude) and excluded Greenland; a total of five ice cores were identified to be located within the Arctic region. Greenland was separated for individual analysis due to the large data collection (n = 11) efforts there. Northern and southern Greenland exhibit differences in seasonal aerosol deposition types and aerosol sensitivities; north Greenland is influenced by high rates of dry deposition during winter months while south Greenland is influenced by high rates of summer wet deposition (Li & Flanner, 2018). Furthermore, differences in mean glacier size and cloud cover fraction between northern and southern Greenland have been shown to produce different snowmelt rates and surface energy fluxes given the same change in aerosol load (Ward et al., 2018). For these reasons, Greenland was divided into two continental regions for this study: north and south. The Greenland divide falls along 71.5° latitude, the median between Greenland's lowest latitude (60.0°) and highest latitude (83.0°). Similarly to Greenland, previous work has suggested that the East and West Antarctic ice sheets can be considered separately because BC deposition between ice sheets can be uncorrelated and each sheet has been observed to have different BC sources (Bisiaux et al., 2012; Stohl & Sodemann, 2010). However, after testing every possible binary regional division of Antarctic ice cores, the maximum mean PD/PI BC ratio difference was 0.1 (Figure S5). In this study Antarctica was therefore kept as a single continuous region for analysis (Figure 2).

To further understand how emission sources have changed, continental region ice core PD/PI BC ratios were compared to local upwind PD/PI BC emission ratios within their local region (Figure 2).

2.3 Climate Model Data

Three ESM ensembles were assembled for analysis: the sixth version of the Climate Model Intercomparison Project (CMIP6), the Large Ensemble Community Project version 1 (LENS), and a subset of CMIP6 simulations from the Community Earth System Model version 2 (CESM2). Data from the CMIP6 historical experiment were used because they provide model data from 1850 to 2014 and represents the most recent IPCC (AR6) assessment. The comparison of CMIP6 ESMs to ice core BC required first identifying those models that provided BC data; seven were identified consisting of CESM2 (Kay et al., 2015), CanESM5 (Swart et al., 2019), MIROC (Kawamiya et al., 2020), EC-Earth3 (Döscher et al., 2022), MRI (Yukimoto et al., 2019), CNRM (Roehrig et al., 2020), and IPSL (Boucher et al., 2020). In addition to contributing to CMIP6, the CESM2 (and sister ESM models based on it) were separately analyzed because they provided additional data on snow and atmospheric burden BC variables (termed sootsn and loadbc, respectively). LENS is an

https://doi.org/10.5194/egusphere-2026-2728
Preprint. Discussion started: 4 August 2026

initial-condition perturbed ensemble of CESM2 simulations initialized with tiny differences in air temperatures (Kay et al., 2015). There is no difference in the CESM2 model versions in any of the LENS ensemble members, so the differences between each run only represent changes in atmospheric transport induced from a perturbed initial condition. Despite only small initial condition differences, some LENS ensemble members have been reported to produce unrealistic temperature profiles (Kay et al., 2015); therefore, comparison of LENS data to ice cores is undertaken with the full LENS ensemble dataset (i.e., no individual LENS ensemble member is isolated for detailed analysis).

Within CMIP6 models, the wet and dry BC deposition variables were the most common, and so deposition forms the main CMIP6 comparison variable under investigation. The only BC indicator available in LENS was aged BC concentrations at the surface. As most ice cores are located far from fire emission sources, we assume that the omission of hydrophobic (or freshly emitted BC) data is minimal in the analysis of LENS data. In addition to comparing all models to each other, 4 model variables within the CESM2 subset were also compared: BC in air column (loadbc), BC in surface air (mmrbc), BC deposition (drybc-wetbc), and BC in snow (sootsn). A complete list of individual models used and the ensembles, subsets, and comparisons they belong to, can be found in Table S5.

The CMIP6 experiment used two emission datasets to prescribe the history of aerosol and gas emissions from PI to PD: a biomass burning emission dataset (van Marle et al., 2017) and an anthropogenic emission dataset (Hoesly et al., 2018). The biomass burning dataset was constructed by combining post-1980 satellite-based estimates of fire emissions from the Global Fire Emissions Database version 4s (GFED4s) with a pre-1980 reconstruction based on the charcoal record, World Meteorological Organization (WMO) visibility observations in South America and Indonesia, and the average of six fire models from the Fire Model Intercomparison Project (FireMIP) (Rabin et al., 2017). The anthropogenic emission dataset was constructed by combining historical fuel use and manufacturing data calibrated against existing emissions inventories, and was organized by year, country, and sector.

2.4 Comparison of the Pre-Industrial and Present Day

The PD/PI BC ratio was calculated using a 25-year mean in each time period (Equation 1 and Figure S3). The data output from ESMs is organized into grid cells using cartesian coordinates and so the PD/PI BC ratio was calculated using the grid cell coordinate that included an ice core's latitude and longitude location. Emissions dataset PD/PI ratios were calculated using an emission mean calculated across each square region as defined in Figure 2 (See Sections 2.2 and 2.5). To represent BC in the surface air, only the surface level concentration was used from the vertically distributed model data. No meaningful difference was found between these methods and alternative grid box averaging or vertical level methods for the LENS ensemble (Tables S6 and S7).

https://doi.org/10.5194/egusphere-2026-2728
Preprint. Discussion started: 4 August 2026

$$\frac{\mathrm{PD}}{\mathrm{PI}} = \frac{\overline{[BC]_{1955-1980}}}{\overline{[BC]_{1850-1875}}} = \frac{\frac{1}{25}\sum_{yr=1955}^{1980}[BC]_{yr}}{\frac{1}{25}\sum_{yr=1850}^{1875}[BC]_{yr}}$$

Equation 1. Definition of the PD/PI ratio where 25-year means are taken around the pre-industrial "PI" (1850-1875) and the present day "PD" (1965-1980). "[BC]" represents the black carbon (BC) analog under investigation (i.e., BC concentration, levoglucosan concentration, or various model BC variables).

To determine if ESM regional means are larger than ice core means globally, a paired T-test was used with "ice core mean > ESM mean" set as the alternative hypothesis. The T-test was reported as significant if the resulting P value was below 0.05 (Virtanen et al., 2020).

2.5 Comparing CMIP6 Biomass Burning vs. Anthropogenic BC Emission Sources

In CMIP6 biomass burning sources are defined as the sum of all natural and anthropogenic open burning fires, while anthropogenic combustion is defined as the sum of fossil fuel, industrial, commercial, and residential burning. All CMIP6 models are forced with biomass burning emissions from van Marle et al. (2017) and anthropogenic emissions from Hoesly et al. (2018). These two CMIP6 emission datasets are used here to compare the contribution of historical estimates of BC from biomass burning and anthropogenic activity to the total BC recorded in alpine ice cores. Data from each emission source (biomass burning or anthropogenic) were converted into PD/PI BC ratios (Equation 1). In many locations anthropogenic PI emissions were lower than 10^{-25} kg m^2 s^{-1}, skewing PD/PI ratios high with such a low dominator (Figure S6). To account for this, while preserving the temporal change in anthropogenic emissions, PI biomass burning emissions were added to both the PD and PI anthropogenic values in results labeled "Anthropogenic+BiomassBurning$_{PI}$" and subsequently compared to the sum of the two datasets labeled "Anthropogenic+BiomassBurning".

3 Results and Discussion

After BC aerosol is emitted to the atmosphere, it undergoes three sequential processes that can result in its preservation in snow and ice layers: transport, deposition, and incorporation in snow and ice layers. Each of these processes is a potential source of disagreement between ESMs and ice core observations; the following results present investigations into each of them. We compare

https://doi.org/10.5194/egusphere-2026-2728
Preprint. Discussion started: 4 August 2026

PD/PI BC ratios from three different sources and to aid comprehension during comparison denote them in the text herein as:

1. Ice cores: PD/PI_{ice}
2. BC emission datasets: PD/PI_{emiss}
3. Global climate / Earth System models: PD/PI_{ESM}

3.1 Change in CMIP6 Biomass Burning vs. Anthropogenic emissions from 1850 CE to 1980 CE

The contributions of CMIP6 emission datasets of anthropogenic, fire (defined as “biomass burning” by CMIP6) and total PD/PI_{emiss} BC ratios were examined individually before investigating simulated ESM BC variables. As to be expected, anthropogenic BC emissions have globally high PD/PI_{emiss} ratios due to the large increases in anthropogenic activity producing BC emissions occurring after 1850 CE (Figure 3). The mean PD/PI_{emiss} ratio in anthropogenic BC emissions is greater than 100 in all six regions analyzed (Figure S7). In contrast, the PD/PI_{emiss} ratio in biomass burning emissions is only greater than a factor of 2 within Equatorial Asia, falling between 0.4 and 1.1 in the Northern Hemisphere and between 0.9 and 2.0 in the Southern Hemisphere (Figure 3). To investigate whether anthropogenic PD/PI_{emiss} BC ratios were being skewed by very low PI values between 1850 CE and 1875 CE, PI biomass burning BC emissions were added to the anthropogenic PD and PI BC emission values individually (Figure 3). The combined BC PD/PI_{emiss} ratio in fire affected regions, including high latitude forests, Central and Southwest Africa, Australia, parts of the Amazon, and Southeast Asia, falls closer to 1 as a result. However, within heavily industrialized, populated, or farmed regions the PD/PI_{emiss} ratio remains greater than 2.

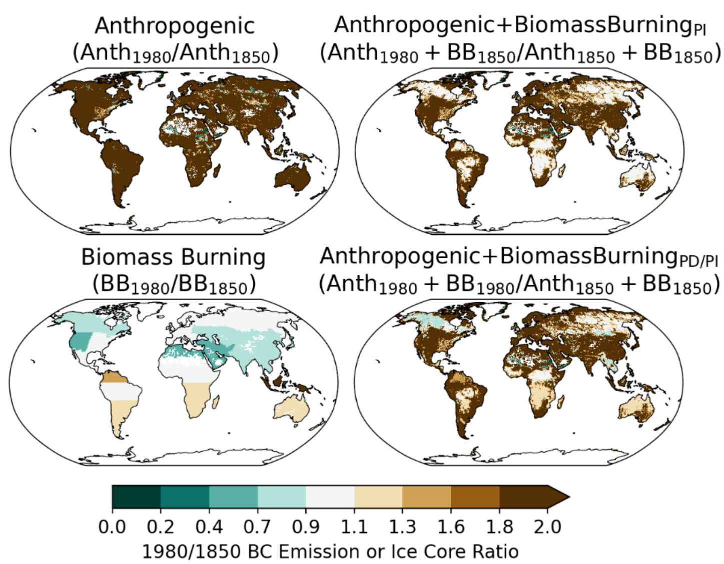

https://doi.org/10.5194/egusphere-2026-2728
Preprint. Discussion started: 4 August 2026

Figure 3. Changes in CMIP6 emission black carbon (BC) data (1980 CE /1850 CE ratios) from anthropogenic (Hoesly et al., 2018) and biomass burning (van Marle et al., 2017) sources (top left and bottom left, respectively), and two combinations of the datasets (bottom right, and top right, respectively). The equations used to calculate each emission dataset's ratio are given in parenthesis above each plot title. Biomass burning ratios all fall below 1.6 while most anthropogenic ratio values are above 2.

To evaluate how CMIP6 BC emission datasets, from biomass burning and anthropogenic combustion sources, compare with BC recorded in ice cores, PD/PI_{emiss} BC ratios were compared with the range of PD/PI_{ice} BC ratios measured from alpine ice cores due to their relative proximity to anthropogenic sources (Figure 4). We assume that changes in emissions of BC from both natural and anthropogenic sources within the vicinity of each alpine core region (Figure 2; local regions) are reasonably captured by the corresponding local ice core record. Although BC may at times be transported away from, rather than toward, the ice core site, we assume that averaging over a 25-year mean across all six sites captures the climatological signal. This comparison therefore serves as a first-order assessment of CMIP6 BC emission dataset performance, prior to the more detailed analyses presented in subsequent sections.

The anthropogenic BC emissions dataset, as well as the combined $Anthropogenic+Biomass_{PD/PI}$ BC emission dataset, both have a mean PD/PI_{emiss} BC ratio greater than 100 (Figures 4 and S7). Anthropogenic BC emission estimates can be expected to have a much lower uncertainty than biomass burning BC emission estimates because PI anthropogenic BC emissions are near zero and PD anthropogenic BC emissions are generally more well documented than historical emissions. One exception to this assumption is biofuel emissions, which were a non-zero BC emission source in the PI. Because the global human population was relatively low in the 19th century (Goldewijk, 2005), biofuel's contribution to uncertainty in Figure 4 is assumed to be small-to-negligible compared to the PD. For biomass burning emissions, PD emissions are expected to have a lower uncertainty than PI emissions because satellite data and other high spatial resolution datasets are more readily available to develop and benchmark emissions against (Chen et al., 2023).

The relatively more well constrained nature of PD/PI_{emiss} anthropogenic BC ratios and biomass burning PD emission values therefore suggests that PI biomass burning emissions are currently underestimated (Figure 4). This conclusion can be come to through the following stepwise analysis:

https://doi.org/10.5194/egusphere-2026-2728
Preprint. Discussion started: 4 August 2026

1. Anthropogenic BC emissions increase several orders of magnitude from the PI to the PD in the emission inventories.

2. Biomass burning BC emissions change very little between the PI and PD, with a mean ratio of ~0.9 across our examined regions.

3. Ice core PD/PI_{ice} BC ratios, which reflect the combined influence of biomass burning and anthropogenic sources, closely resemble the derived ratio from the biomass burning emission dataset.

4. When taken together, the relatively small change in PI to PD biomass burning emissions is insufficient to reconcile the total PD/PI_{emiss} BC emission change with the measured PD/PI_{ice} ratio range from alpine ice cores. This implies that PI biomass burning emissions are highly likely to be underestimated.

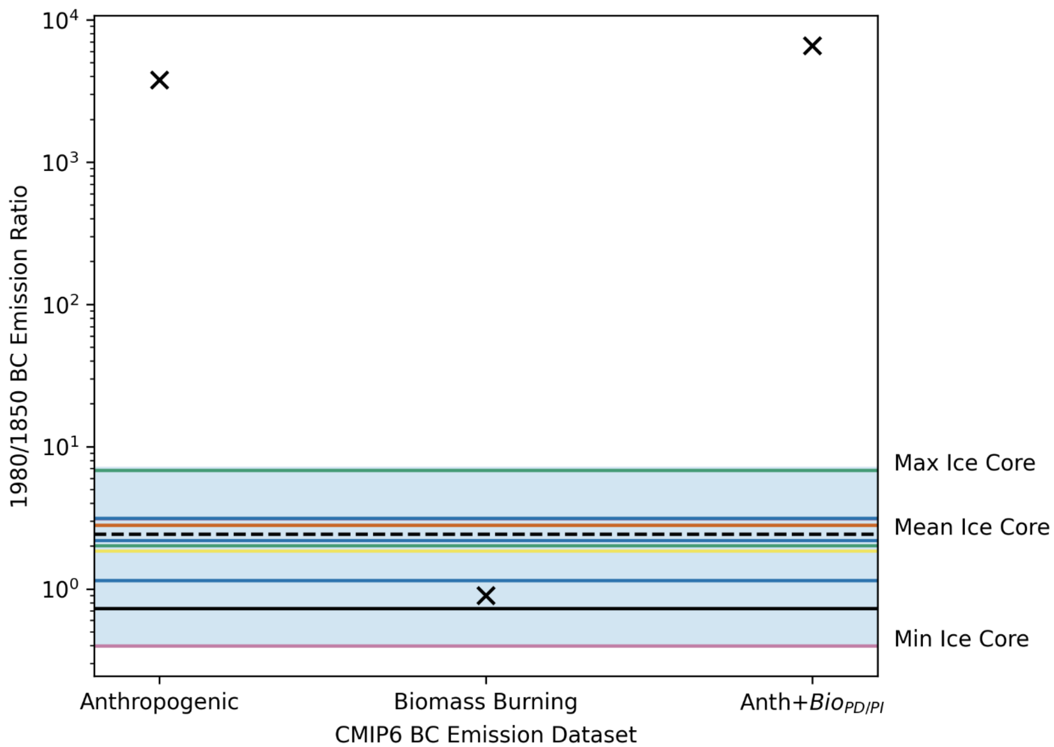

Figure 4. Comparison of CMIP6 anthropogenic and biomass burning black carbon (BC) emission dataset present day (PD; 1980 CE) / pre-industrial (PI; 1850 CE) ratios relative to ice core PD/PI_{ice} BC ratios in the near vicinity. Each X represents the spatial mean of the CMIP6 modeled BC PD/PI_{ESM} emission ratio calculated across all the bounding boxes in the vicinity of an alpine ice core region (Figure 2). Horizontal colored lines represent individual alpine ice core ratios with the line's color matching the bounding box color in Figure 2. Light blue shading represents the minimum to maximum range across all six examined alpine ice core regions.

https://doi.org/10.5194/egusphere-2026-2728
Preprint. Discussion started: 4 August 2026

3.2 CMIP Models Overestimate PD/PI BC Ratios in Nearly Every Region of the World

The previous section investigated CMIP6 emission datasets and analysis herein shifts to simulated BC variables within ESMs. A comparison of BC ice core ratios to emission dataset ratios does not account for the aerosol transport and depositional processes that will alter the PD/PI$_{ESM}$ ratios in downstream ESM variables. To understand if either transport or depositional processes alter the result found in the emissions datasets that PI fire emissions are too low, CMIP6 and LENS (CMIP5) modeled PD/PI$_{ESM}$ BC deposition ratios were compared to ratios obtained from the ice cores, producing a clear result that both CMIP6 and LENS models overestimated the PD/PI$_{ESM}$ BC ratio in nearly every region of the world (Figure 5).

Globally, the mean PD/PI$_{ice}$ BC ratio across all ice cores is 1.55 while model ratios are significantly higher: CMIP6 PD/PI$_{ESM}$ ratio = 3.08 and LENS PD/PI$_{ESM}$ BC ratio = 5.80. Furthermore, CMIP6 medians and means in 30/37 ice cores analyzed are above the ice core inter quartile range, both CMIP6 and LENS's modeled ratios at many ice core locations are above 3, and in many regions the lowest modeled ratio is higher than the highest ice core ratio. The difference between ESM results and ice core data is statistically significant at the global scale and supports the hypothesis that PI fire emissions are currently underestimated across CMIP experiments.

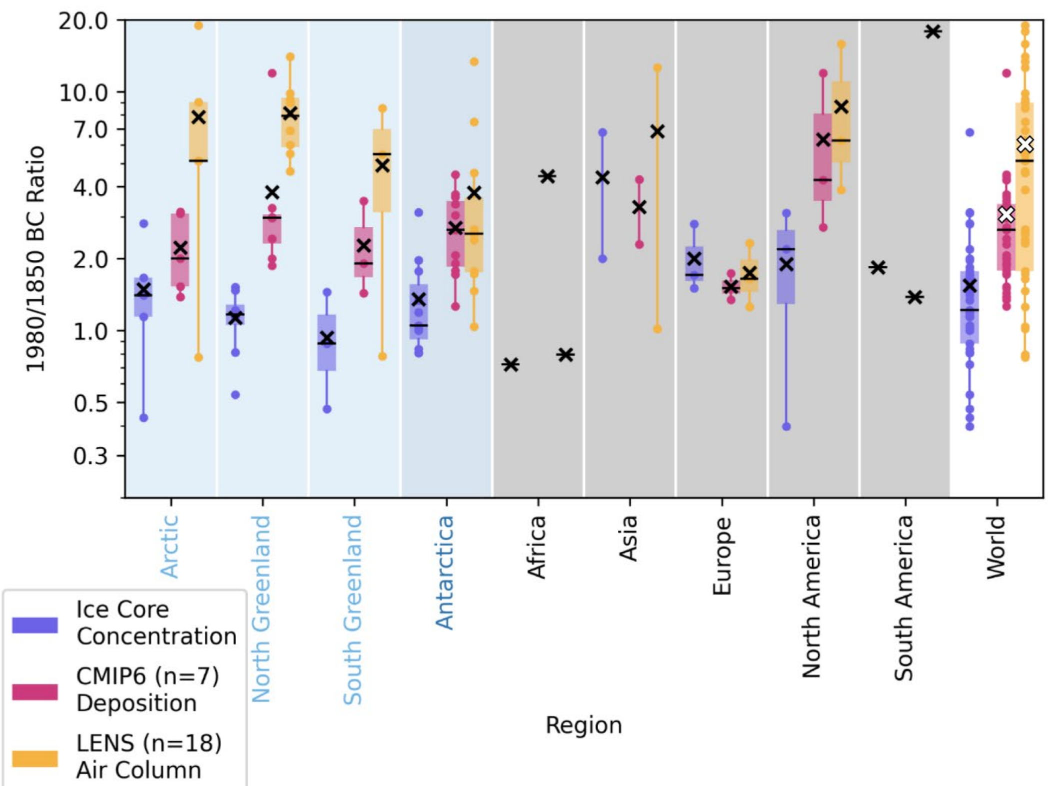

https://doi.org/10.5194/egusphere-2026-2728
Preprint. Discussion started: 4 August 2026

Figure 5. Modeled and observed pre-industrial / present day (1980 CE/1850 CE) black carbon (BC) ratios across different regions of the world. The ice core ratio is based on measured BC concentrations within each set of cores, the CMIP6 ratio is based on simulated BC deposition fluxes from both natural and anthropogenic sources, and the LENS ratio is based on the simulated BC column burden from both natural and anthropogenic sources. Each data point represents either a measured ice core PD/PI_{ice} ratio or the modeled PD/PI_{ESM} ratio within the grid cell containing an ice core's location. Medians, means, and data points are represented by black horizontal lines, X's, and colored points, respectively. Whiskers extend to the farthest data point within 1.5 times the inter-quartile range. Background bar colors denote if the region is in the Arctic, Antarctic, or neither (light blue, dark blue, and grey, respectively). Regions with two data points show only the two points connected by a line and their mean value. Regions with a single data point are represented by a colored X and a black line. Global model mean X's are internally colored white to highlight a statistically significant difference ($P<0.05$) between model and ice core means.

In North Greenland, ice core BC ratios have a PD/PI_{ice} mean and median of 1.13 and 1.17, respectively, and a narrow first to third quartile range of 1.06 to 1.28. CMIP6 and LENS have much larger North Greenland PD/PI_{ESM} BC ratio medians of 2.96 and 7.94, respectively, resulting in no modeled BC ratio falling within North Greenland ice core's first to third quartile range of the ice cores or overall range (0.54 to 1.52). In South Greenland, ice core PD/PI_{ice} BC ratios have slightly lower PD/PI mean and median ratios compared to their northern counterparts at 0.93 and 0.88, respectively, and a narrow first to third quartile range of 0.68 to 1.17. CMIP6 and LENS have much larger mean and median PD/PI_{ESM} ratios at 4.93 and 5.48, respectively, resulting in only one single modeled ratio in LENS falling within the ice cores first to third quartile range. Both ice core and model data exhibit lower ratios in South Greenland compared to North Greenland. Greenland's latitude-based differences in ice core PD/PI_{ice} ratios can be further seen in Figure S8 where PD/PI_{ice} ratios have a weak correlation with latitude of $R^2 = 0.24$, agreeing with previous findings that a latitude based difference in Greenland's BC aerosol deposition seasonality and sensitivity likely exists (Li & Flanner, 2018; Ward et al., 2018).

In the Arctic, which consists of the 5 remaining ice core locations that are both above the Arctic circle and outside of Greenland, PD/PI_{ice} ratios have a mean and median value of 1.49 and 1.41, respectively, a range from 0.43 to 2.82, and a first to third quartile range from 1.14 to 1.67. Although not as inflated as Greenland, CMIP6 mean and median PD/PI_{ESM} ratios are once more above ice core values at 2.23 and 2.00, respectively, with 2/5 CMIP6 ratios falling within the ice core first to third quartile range. LENS displays a larger range in the Arctic than in any other examined region with a min and max ratio of 0.77 and 19.02, respectively, representing a factor of 25 uncertainty across ensemble simulations. The large range observed in the Arctic represents the potential for transport deviations created by tiny initial temperature differences (Section 3.4) rather than any unique property of the Arctic (Figure S9).

https://doi.org/10.5194/egusphere-2026-2728
Preprint. Discussion started: 4 August 2026

Although Antarctica represents BC deposition from different Southern Hemisphere source regions, the differences between ice core and model ratios are similar to those found in the Arctic regions. Antarctic ice cores have PD/PI_{ice} ratio means and medians of 1.36 and 1.05, respectively, and a first to third quartile range from 0.92 to 1.56, respectively. CMIP6 has one PD/PI_{ESM} ratio within the ice core range, and a mean and median ratio of 2.70 and 2.64, respectively. LENS shows 2 PD/PI_{ESM} ratios within the Antarctic ice core range and 3.78 and 2.54 for its mean and median, respectively. The general similarity in the ice core-model differences of Antarctica and the Arctic regions suggests that there is a global fire emission bias.

Alpine ice core records are sparse with fewer sites per region compared to their polar counterparts. Alpine ice cores show more varied ratios than at high latitudes. In Africa, where only a single ice core record was available, the CMIP6 and LENS PD/PI_{ESM} ratio is 4.42, and 0.80, respectively, compared to the ice core value of 0.72. Asia is one of two regions that show good agreement between ice core and model ratios. Asian ratio means for CMIP6, LENS, and ice cores are 3.29, 6.83, and 4.51, respectively (we do not calculate the ratio median in Asia because only two ice cores are available). Europe is the second region with good agreement and means of 1.53, 1.74, and 2.0 for CMIP6, LENS, and ice core records, respectively. In North America, ice cores in the region have a first to third quartile range of 1.29 to 2.65, while CMIP6 and LENS have median values much higher at 6.31 and 8.67, respectively. In South America, the single ratio for the ice core record, CMIP6, and LENS are 1.84, 1.39, and 17.93, respectively. Overall, the CMIP6 and LENS in Europe and CMIP6 alone in South America are only regions where modeled medians are lower than ice core values.

Changes in land use from the PI to PD can possibly help explain the range of alpine ice core-model ratio differences. By 1850 CE, Europe had already experienced much of the land use transition that was likely responsible for many of the high PI BC ice core values in other regions (Kaplan et al., 2017). In contrast, extensive colonial land clearing in North America resulted in increased combustion during the PI period (Ryan et al., 2013). The timing of European and North American land use transitions suggests that the human modification of fire regimes is a key process to include in reconstructing fire emission datasets.

Results in Figure 5 support previous findings, including that CMIP6 underestimated historical fire emissions (Hamilton et al., 2018; Liu et al., 2021; Moseid et al., 2022; Zhang et al., 2024), that there is a 1901 CE to 1978 CE decrease in fire (Guo et al., 2025), as well as a post-1850 CE North American decline in fire found in inverse modeling studies (Eckhardt et al., 2023; Guo et al., 2025).

3.3 Comparison of Aerosol Concentration and Deposition PD/PI ratios

When suspended in the atmosphere, BC has a residence time of between a few days to a couple of weeks (Cape et al., 2012). During its atmospheric lifetime BC can be chemically transformed, including transitioning from an initial hydrophobic phase to a hydrophilic one, and transported long distances by several mechanisms such as low altitude transport, transport with ascent at the Arctic front, or ascent at the emission source (Stohl, 2006). Ultimately, all BC aerosol

https://doi.org/10.5194/egusphere-2026-2728
Preprint. Discussion started: 4 August 2026

emitted to the atmosphere is deposited back to the Earth's surface through either wet deposition, involving precipitation, or dry deposition, involving gravitational settling, Brownian motion, impaction, or interception (Seinfeld & Pandis, 2016). Uncertainty in BC concentrations therefore lies not only in the uncertainty of each of these post-emission aerosol processes (Browse et al., 2012), but also in how these processes may have changed over time, and ESM abilities to simulate them and their change.

To investigate how individual modeled aerosol processes relate to the discrepancy between modeled and observed ratios, a series of key aerosol process variables from the CESM2 (a subset of CMIP6) were investigated (Figure 6). CESM2 is used because it was the only CMIP6 model dataset that contained each of the 4 variables under investigation: (1) BC in air column (model variable name: loadbc); (2) BC in surface air (model variable name: mmrbc); (3) BC deposition (model variable names: drybc and wetbc); and (4) BC in snow (model variable name: sootsn). Their presented order in Figure 6 corresponds to how closely each variable is generally expected to physically represent BC measured within an ice core, where BC in the air column is the furthest and BC in snow is the closest to BC in an ice core (Table S8). It should be noted however that the CMIP6 variable "sootsn" (i.e., BC in snow) is defined as "soot_content_of_surface_snow" (van den Hurk et al., 2016) and so this variable does not directly correspond to measurements of ice core BC because firn densification processes can alter BC concentrations by up to three orders of magnitude between fresh snow and granulated ice (Kang et al., 2020; Schmitt et al., 2019; Xu et al., 2012). As densification rates depend on the rate of snow precipitation (Herron & Jr, 1980), BC ratios can further change because of differing PD and PI rates across regions (Zuo & Qian, 2022).

In general, median PD/PI_{ESM} CESM2 ratios from BC in the air column, BC deposition to snow, BC in surface air, and BC in snow are all more similar to each other than to the ice core ratio (Figure 6). Regional ice core PD/PI_{ice} ratio medians range from 1.05 to 1.93 and the corresponding values from model variables are 1.91 to 3.90. A complete list of medians is given in Table S8. Every model variable's median PD/PI_{ESM} ratio in every region is above the ice core's PD/PI_{ice} third quartile in the corresponding region. All variable means except BC in snow are significantly ($P<0.05$) larger than ice core values in polar regions, and BC in air column is also significantly larger in alpine regions. BC in air column and BC in surface air show median ratios with each other's first to third quartile range in the North Pole and South Pole, while BC deposition to snow and BC in surface air share that property in alpine regions. In the North Pole and South Pole, modelled variables show the same relative relationship where BC deposition to snow, BC in air column, BC in surface air, and BC in snow have decreasing ratio medians in that order. Figures S10 and S11 show ratios between modeled variables across the globe.

To date, previous studies have generally investigated the spatial-temporal variability associated with the magnitude of "in air" model variables separately from "in snow" model variables. The most representative variable to ice core BC in CMIP6 models could be argued to be sootsn, but the uncertainty in CMIP6 sootsn has only been evaluated by two studies. Chen et al. (2022) found that spatial-temporal patterns of CMIP6 sootsn agreed well with snow BC concentration observations from 1980 to 2014, with generally increasing trends over the study

https://doi.org/10.5194/egusphere-2026-2728
Preprint. Discussion started: 4 August 2026

period, although there were considerable disagreements between models (CESM2, CESM2-FV2, CESM2- WACCM, CESM2- WACCM-FV2, NorESM2-LM, NorESM2-MM, and TaiESM1), especially in Europe and Asia which showed standard deviations of 200 ng g^{-1} (corresponding to a relative standard deviation of 300%). Chen et al. (2024) found that CMIP5 and CMIP6 models struggled to reproduce inter decadal variability in global snow BC concentrations, especially in Antarctica where CMIP6 overestimated snow BC radiative forcing by 144%. The authors identified post-depositional snow processes as the primary sources of large-scale model errors, rather than other land components of models, which show good agreement with observations (Chen et al., 2024; Ma & Wang, 2024).

Although BC in snow is the only variable that is not significantly ($P<0.05$) greater than ice core ratios, it is not as well evaluated as BC in the air column, and can contain downstream uncertainties from other processes such as meteorology (Zhang et al., 2022). Additionally, BC in snow is only available in model grid cells that have a substantial fraction of their landcover covered in snow, which is why the variable has fewer datapoints in all three regions shown in Figure 6. For these reasons, BC in snow may not actually represent a good agreement between ice cores and ESMs. These sources of uncertainty can explain some of the difference between sootsn and the other model variables, but the persistent discrepancy between all four model variables and the ice core values in each of the hemispheric regions supports the proposition that the major bias lies in fire emission datasets rather than any physical process being modeled by an ESM.

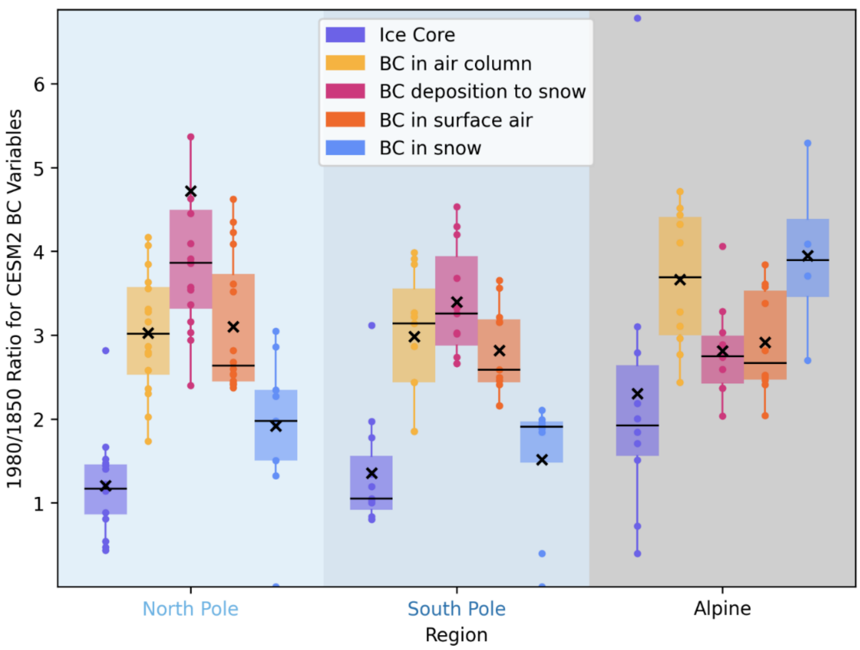

Figure 6. Simulated PD/PI_{ESM} black carbon (BC) variable ratios from CESM2 compared to measured ice core BC PD/PI_{ice} ratios. Each data point represents either an observed or modeled

https://doi.org/10.5194/egusphere-2026-2728
Preprint. Discussion started: 4 August 2026

PD/PI BC ratio at one ice core's location in one of three regions. Medians, means, and data points are represented by black horizontal lines, black Xs, and colored points respectively. The box represents the range from the first quartile to the third quartile, and the whiskers extend to the farthest data point within 1.5 times the inter-quartile range.

3.4 Influence of Transport on Modelled Deposition Ratios

An alternative explanation for the discrepancy between modeled and ice core BC ratios is that BC atmospheric transport pathways, from aerosol emission to deposition, over the Industrial era are significantly different from what is being simulated by ESM models. To explore the role of aerosol transport we used the LENS ensemble (Figure 7). LENS is an ensemble of CESM2 runs, identical in all respects except for a very small variation in the initial atmospheric temperature on the order of 10^{-14} K. These small perturbation to the initial condition results in variations in meteorology (Kay et al., 2015), and therefore in aerosol transport pathways. Combined, the 17 LENS ensemble members can then be used to describe the possible distribution of potential transport pathways and assess how differences in transport may affect PD/PI_{ESM} BC ratios.

We found that there was limited agreement between the LENS ensemble-mean BC ratio and the ice core BC ratio (Figure 7, top panel and third row). Only three of the 37 ice core locations fall within ±0.25 (absolute ratio difference) of the ensemble-mean LENS values, underscoring the extent to which the ensemble mean fails to reproduce the spatial variability captured in the ice core record. Examination of individual ensemble members (fourth to last columns) shows that members #19 and #25 yield ratios most similar to the ice core values. However, even for these members, substantial discrepancies remain: 7/37 and 6/37 locations, respectively, exhibit BC ratios exceeding 9.0, well above the maximum observed ice core ratio of 6.8. Thus, even the ensemble members exhibiting the closest overall agreement systematically overestimate BC ratios at a significant fraction of sites. This behavior implies that discrepancies are unlikely to be resolved by either averaging across internal transport variability or identifying one single "optimal" transport ensemble member alone.

The symmetric bias factor (SBF) analysis reinforces this conclusion (Figure 7; bottom vertical bar). Across the LENS individual runs, only a limited fraction (18.2%) of site–ensemble comparisons fall within the low-bias category ($|SBF| \leq 0.5$, approximately within a factor of two). Conversely, a substantial proportion (70.3%) instead lies in the high ($|SBF| > 1$) bias category, indicating deviations exceeding a factor of three at least. Notably, high-bias cases are dominated by positive SBF values, consistent with the prevalence of ratios exceeding the observational upper bound.

Taken together, the raw ratio comparisons and SBF distribution demonstrate that the mismatch is not confined to a few extreme outliers but rather reflects a systematic tendency toward elevated simulated PI to PD BC ratios across the LENS ensemble relative to the ice core record. The spread of the ensemble therefore appears to represent internal aerosol transport variability superimposed on an underlying structural bias, rather than variability centered on the observational constraint. In other words, while individual LENS ensemble members do occasionally approach

https://doi.org/10.5194/egusphere-2026-2728
Preprint. Discussion started: 4 August 2026

observational values at specific sites, the ensemble as a whole does not bracket the observational constraint.

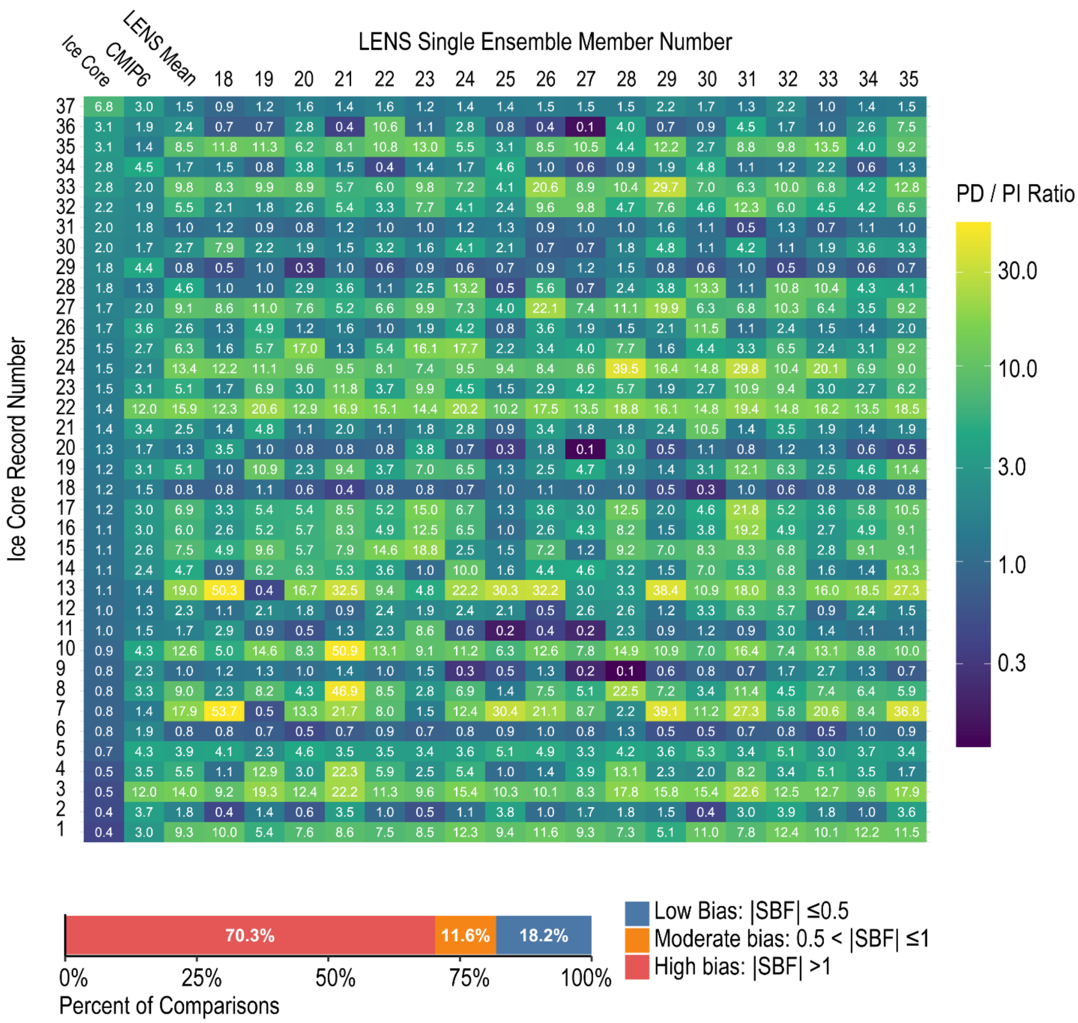

Figure 7. Heatmap comparing the pre-industrial (1850 CE) to present day (1980 CE) change in black carbon between the 17 LENS transport scenarios investigated (18 through 35) and ice core data (top; ice core data shown in the left most column with modeled data to the right). Also included is the CMIP6 mean (Figure 5) and the LENS ensemble mean. Rows are sorted by ice core indexes defined in Figure 1. Summary of bias between ice core observation (O) and 17 ensemble models (M) (bottom). Bias categories are defined using an absolute symmetric bias factor (|SBF|) metric: |SBF| = |O/M −1| (or the symmetric equivalent). |SBF| ≤ 0.5 corresponds approximately to

https://doi.org/10.5194/egusphere-2026-2728
Preprint. Discussion started: 4 August 2026

agreement within a factor of two; $0.5 < |SBF| \leq 1$ corresponds to deviations between factors of two and three; $|SBF| > 1$ corresponds to deviations greater than approximately a factor of three.

3.5 Defining the Pre-Industrial End Year

Previous work has shown that altering the definition of what constitutes "the PI" changes the probability of the world meeting goals like the Paris Climate accord. For example, the chance of exceeding 1.5°C warming by 2100 varies between 61% to 88% when the amount of late nineteenth century's warming varies by 0.2°C (Schurer et al., 2017). However, the effect of choice in what year is used to define the PI on fire emissions, and the related aerosol forcing baseline, has yet to be explored.

The probability distributions in Figure 8 show that as the PI definition year increases from 1750 CE to 1900 CE the median PD/PI_{ice} BC ratio varies in response. Two trends become apparent as the definition of PI year moves closer to the PD: (1) the relative probability distribution narrows, indicating more constrained values; and (2) ratio values greater than 1 become more frequent for pre-20th century definitions of the PI, confirming that fire regimes experienced large-scale changes between 1750 CE and 1850 CE (Barker et al., 2021; Brugger et al., 2021; Chellman et al., 2017; Knorr et al., 2014; Legrand & De Angelis, 1996; McConnell et al., 2007; Thevenon et al., 2009; Whitehair et al., 2018; Whitlow et al., 1994; Zhang et al., 2024). As climate warming can be assumed to be insignificant during this time, the change can be more readily attributed to land use and land cover change than shifts in fire weather. One other important point to note is that when using 1900 CE as the PI reference year the ratio peak shifts to become more similar to the 1750 CE distribution peak, likely due to an Industrial era BC increase in both biofuel and industrial emissions in the early decades of the 20th century (Faïn et al., 2025; Guo et al., 2025; Hamilton et al., 2018; Liu et al., 2021; Moseid et al., 2022; Zhang et al., 2024). While not evident in the global mean ice core analysis, the influence of such peaks varies regionally due to differences in the timing of industrialization. For example, parts of Western Europe such as the United Kingdom were already highly industrialized by around 1850 CE, whereas industrialization across much of Asia occurred later within the 20th century, altering the timing and magnitude of BC increases recorded in alpine ice core data (e.g. Kaspari et al., 2020).

Different definitions of the PI represent different BC (and other co-emitted species) baselines for radiative forcing estimates. Although the exact definition of the PI does change ice core PD/PI ratios, these changes are smaller than differences in simulated PD/PI_{ESM} ratios (Figure 5) and thus do not alter the overall conclusion that PI fire emissions are underrepresented in current CMIP emission datasets.

https://doi.org/10.5194/egusphere-2026-2728
Preprint. Discussion started: 4 August 2026

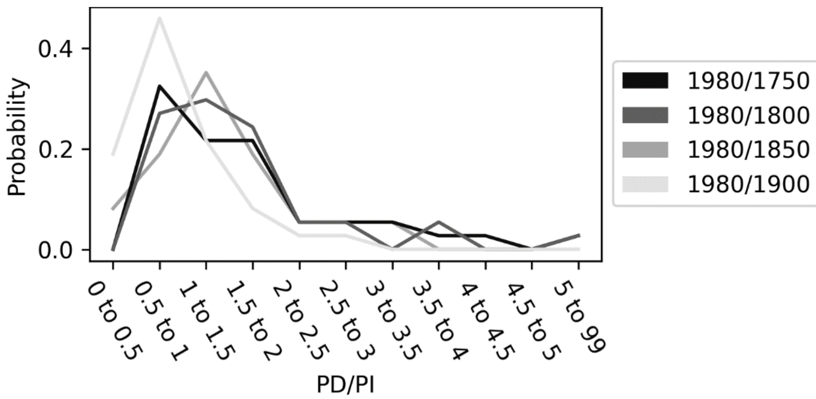

Figure 8. Differences in the distributions of ice core PD/PI_{ice} ratios based on the definition of the PI year.

4 Improving Fire Emission Reconstructions

For models to better reproduce the PI to PD change in BC observed in ice cores, the major processes involved in moving BC aerosol from emission source to final deposition location need to be understood at a higher level of detail than present. Here we highlight three sources of uncertainty to be reduced that can improve the simulation of fire BC (and other co-emitted aerosol) over the historical period: (1) aerosol properties; (2) deposition processes; and (3) post-deposition processes.

The main conclusion of this work is that the sources of global BC, namely fire compared to industrial combustion, have changed significantly from the PI to the PD. In the case of fire this change is a reduction from the PI to the PD, a trend that is counter to current and past CMIP emission datasets. In addition to changing the aerosol burden, the physicochemical properties of BC have likely also changed over the Industrial Era. How such changes to aerosol properties then propagate to variations in aerosol transport and deposition location, over time, remains relatively unknown. Several physicochemical properties of aerosol, including particle size, hygroscopicity, optical properties, and chemical makeup, can depend on the source of the aerosol (Blanco-Donado et al., 2022; Liu et al., 2022). A shift in aerosol properties can then alter aerosol transport distance (Seinfeld & Pandis, 2016). For example, in the Community Atmosphere Model version 6 (CAM6)'s Modal Aerosol Module (MAM4) BC aging has been suggested to be too fast when compared to experimental results, resulting in overestimates of surface BC concentration in some regions, and conversely, underestimates in others (Shen et al., 2023). If BC aerosol ages quickly, and precipitates out nearer to source, it may not reach higher latitudes (Browse et al., 2012). The question would then be if the hygroscopicity or the aging rate of BC has changed over time, and how such changes may alter results presented here if not adequately captured by models.

Deposition, where aerosol settles out of the air back to the surface, either through wet or dry deposition processes, is a key uncertainty in climate modelling. Dry deposition describes four processes (gravitational settling, impaction, interception, and Brownian motion) as opposed to the precipitation based scavenging processes that define wet deposition (Liu et al., 2020; Seinfeld &

https://doi.org/10.5194/egusphere-2026-2728
Preprint. Discussion started: 4 August 2026

Pandis, 2016). Climate models parameterize these processes to make them computationally efficient, with the exact parameterization evolving over time. However, aerosol deposition measurements are challenging to acquire, especially on the spatial and temporal scales needed for ESM parameterization constraints (Farmer et al., 2021). This can lead to potential overestimates in the deposition of accumulation and Aitken mode particles and/or underestimates of coarse mode deposition (Emerson et al., 2020). Changing deposition rates also affects atmospheric aerosol lifetimes, with the most pronounced effects often simulated in remote polar regions (Vignati et al., 2010a).

When BC aerosol deposition occurs over a glaciated region, BC deposited on the seasonal snowpack or on glacier surfaces can undergo post-depositional processes. During this transition, melting, sublimation, and the re-freezing of ice can all lead to vertical redistribution of BC particles relative to the surrounding ice pack (Ginot et al., 2001; Liou et al., 2011; Schwarz et al., 2013). Multiple studies have found that surface snow melt and runoff can increase the concentration of hydrophilic BC particles at the surface of ice cores and at the bottom of the snowpack (Doherty et al., 2013; Ginot et al., 2014; Xu et al., 2012). Under high BC concentrations, migration to the bottom of the snowpack dominates (Conway et al., 1996). Post-depositional processes can alter BC concentrations within melt seasons by between a factor of 5 to 10 (Doherty et al., 2013; Xu et al., 2012). However, even when significant post-depositional processes occur, temporal trends in ice core BC timeseries remain primarily driven by source emission changes because vertical migration is largely limited to the uppermost layers of snow (Osmont et al., 2018). Despite the body of literature investigating post-depositional processes, no CMIP6 ESM includes any post-depositional processes for BC deposited to snow. Current analytical methodology used to measure BC concentrations cannot differentiate differences in the physical properties of BC particles that may give insight into their source type (McConnell et al., 2007). To help overcome this, some studies have used alternative or additional methodologies to help identify the sources of BC in ice core records. Jenk et al. (2006) analyzed samples from an alpine ice core using radiometric techniques to quantify the relative amount of anthropogenic and biomass burning Elemental Carbon (EC) and organic carbon (OC). They found that the fraction of anthropogenic EC and OC grew significantly from 1870 CE to 1980 CE, with unexpectedly high anthropogenic fractions of pre-1850 EC values consistently near 50% and attributed to contributions from mineral dust. Wang et al. (2025) used radiocarbon analysis of a Himalayan ice core and found that the anthropogenic fraction of BC has decreased slightly from 76 to 70% from 1990 to 2012, while the biomass burning fraction was highly correlated with South Asian fires. Despite the existence of viable techniques, as shown in these two studies, these additional source characterization steps are rare, making a global analysis of trends challenging.

5 Conclusions

We compared 36 ice core records of BC and 1 record of levoglucosan, covering all continents except Oceania, to ESM model simulations of BC at ice core locations. We found that the PI to PD BC ratio simulated by ESMs, using either the CMIP5 or the CMIP6 BC emission inventories,

https://doi.org/10.5194/egusphere-2026-2728
Preprint. Discussion started: 4 August 2026

were overestimated compared to ice cores. Globally, simulations of BC change are significantly ($P<0.05$) larger than ice core measurements. Regionally, the multi-model mean PI to PD BC ratio was found to be outside of the inter-quartile range of the corresponding ice core PI to PD BC ratio in three quarters of polar regions (3 out of 4) and two-thirds of continental regions (6 out of 9). We explored three sources of possible model-observation discrepancy: emission, transport, and aerosol processes, finding that an underestimate of PI fire emissions in CMIP emission inventories to be the primary reason for model-observation discrepancies.

Our results call for continued efforts to reevaluate fire emission data, especially given the importance of aerosol for future radiative forcing estimates within CMIP or related activities such as AerChemMIP. To aid this initiative we present four areas of potential future development:

1. Continued reevaluation of pre-industrial to present-day fire emission inventories, including multiple paleoenvironmental archives (e.g., ice cores, tree rings, charcoal, speleothems).
2. Inclusion of post-depositional aerosol processes in cryosphere components of future ESM development.
3. The constraint of fire models with ice core (and ideally other records of burning) data in coupled ESM simulations.
4. Further develop, and expand the use of, methodology that can identify anthropogenic vs. biomass burning BC aerosol in ice core records (e.g., Jenk et al., 2006; Wang et al., 2025).

Acknowledgements

We would like to acknowledge Viney Aneja, Adrianna Foster, and Srijan Sengupta for their committee support of NLB and helpful comments on the study as it developed. All software analysis and figure composition were performed in either Bash or Python, and mainly used the following software packages: netCDF Operators (NCO) (Zender, 2008), Climate Data Operators (CDO) (Schulzweida, 2023), Matplotlib (Hunter, 2007), Cartopy (Elson et al., 2024), InterpolateScalingPy (Liefeld, 2025), Numpy (Harris et al., 2020), and Scipy (Virtanen et al., 2020). We would like to acknowledge high-performance computing support from the Derecho system (doi:10.5065/qx9a-pg09) provided by the NSF National Center for Atmospheric Research (NCAR), sponsored by the National Science Foundation. Any use of trade, firm, or product names is for descriptive purposes only and does not imply endorsement by the U.S. Government.

Author Contributions

CS, KC, DSH designed the study. NK, CB, EB, PG, RZ, LT and SK provided data. NLB and DSH analyzed data. NLB and DSH drafted the manuscript which was then developed and edited by all authors. NLB developed all Figs except Figure 7 developed by DSH.

Open Research

https://doi.org/10.5194/egusphere-2026-2728
Preprint. Discussion started: 4 August 2026

All data used in this study are publicly available. Table S3 lists all ice core publications. Table S9 incorporates all data used in the publication.

References

Ackerman, A. S., Toon, O. B., Stevens, D. E., Heymsfield, A. J., Ramanathan, V., & Welton, E. J. (2000). Reduction of Tropical Cloudiness by Soot. *Science*, *288*(5468), 1042–1047. https://doi.org/10.1126/science.288.5468.1042

Amiridis, V., Giannakaki, E., Balis, D. S., Gerasopoulos, E., Pytharoulis, I., Zanis, P., et al. (2010). Smoke injection heights from agricultural burning in Eastern Europe as seen by CALIPSO. *Atmospheric Chemistry and Physics*, *10*(23), 11567–11576. https://doi.org/10.5194/acp-10-11567-2010

Andela, N., Morton, D. C., Giglio, L., Chen, Y., van der Werf, G. R., Kasibhatla, P. S., et al. (2017). A human-driven decline in global burned area. *Science*, *356*(6345), 1356–1362. https://doi.org/10.1126/science.aal4108

Andersen, K. K., Svensson, A., Johnsen, S. J., Rasmussen, S. O., Bigler, M., Röthlisberger, R., et al. (2006). The Greenland Ice Core Chronology 2005, 15–42ka. Part 1: constructing the time scale. *Quaternary Science Reviews*, *25*(23–24), 3246–3257. https://doi.org/10.1016/j.quascirev.2006.08.002

Andreae, M. O., & Rosenfeld, D. (2008). Aerosol–cloud–precipitation interactions. Part 1. The nature and sources of cloud-active aerosols. *Earth-Science Reviews*, *89*(1), 13–41. https://doi.org/10.1016/j.earscirev.2008.03.001

Aragão, L. E. O. C., Anderson, L. O., Fonseca, M. G., Rosan, T. M., Vedovato, L. B., Wagner, F. H., et al. (2018). 21st Century drought-related fires counteract the decline of Amazon deforestation carbon emissions. *Nature Communications*, *9*(1), 536. https://doi.org/10.1038/s41467-017-02771-y

Archibald, Nickless, A., Govender, N., Scholes, R. J., & Lehsten, V. (2010). Climate and the inter-annual variability of fire in southern Africa: a meta-analysis using long-term field data and satellite-derived burnt area data. *Global Ecology and Biogeography*, *19*(6), 794–809. https://doi.org/10.1111/j.1466-8238.2010.00568.x

Archibald, Staver, A. C., & Levin, S. A. (2012). Evolution of human-driven fire regimes in Africa. *Proceedings of the National Academy of Sciences*, *109*(3), 847–852. https://doi.org/10.1073/pnas.1118648109

Arora, V. K., & Melton, J. R. (2018). Reduction in global area burned and wildfire emissions since 1930s enhances carbon uptake by land. *Nature Communications*, *9*(1), 1326. https://doi.org/10.1038/s41467-018-03838-0

Baker, J. C. A., & Spracklen, D. V. (2019). Climate Benefits of Intact Amazon Forests and the Biophysical Consequences of Disturbance. *Frontiers in Forests and Global Change*, *2*. https://doi.org/10.3389/ffgc.2019.00047

https://doi.org/10.5194/egusphere-2026-2728
Preprint. Discussion started: 4 August 2026

Barker, J. D., Kaspari, S., Gabrielli, P., Wegner, A., Beaudon, E., Sierra-Hernández, M. R., & Thompson, L. (2021). Drought-induced biomass burning as a source of black carbon to the central Himalaya since 1781 CE as reconstructed from the Dasuopu ice core. *Atmospheric Chemistry and Physics*, *21*(7), 5615–5633. https://doi.org/10.5194/acp-21-5615-2021

Bellouin, N., Quaas, J., Gryspeerdt, E., Kinne, S., Stier, P., Watson-Parris, D., et al. (2020). Bounding Global Aerosol Radiative Forcing of Climate Change. *Reviews of Geophysics*, *58*(1), e2019RG000660. https://doi.org/10.1029/2019RG000660

Bender. (2002). Orbital tuning chronology for the Vostok climate record supported by trapped gas composition. *Earth and Planetary Science Letters*, *204*(1), 275–289. https://doi.org/10.1016/S0012-821X(02)00980-9

Bender. (2020). Aerosol Forcing: Still Uncertain, Still Relevant. *AGU Advances*, *1*(3), e2019AV000128. https://doi.org/10.1029/2019AV000128

Bender, Sowers, T., Barnola, J.-M., & Chappellaz, J. (1994). Changes in the O2/N2 ratio of the atmosphere during recent decades reflected in the composition of air in the firn at Vostok Station, Antarctica. *Geophysical Research Letters*, *21*(3), 189–192. https://doi.org/10.1029/93GL03548

Bender, Barnett, B., Dreyfus, G., Jouzel, J., & Porcelli, D. (2008). The contemporary degassing rate of ^{40} Ar from the solid Earth. *Proceedings of the National Academy of Sciences*, *105*(24), 8232–8237. https://doi.org/10.1073/pnas.0711679105

Bisiaux, M. M., Edwards, R., McConnell, J. R., Curran, M. a. J., Van Ommen, T. D., Smith, A. M., et al. (2012). Changes in black carbon deposition to Antarctica from two high-resolution ice core records, 1850–2000 AD. *Atmospheric Chemistry and Physics*, *12*(9), 4107–4115. https://doi.org/10.5194/acp-12-4107-2012

Blanco-Donado, E. P., Schneider, I. L., Artaxo, P., Lozano-Osorio, J., Portz, L., & Oliveira, M. L. S. (2022). Source identification and global implications of black carbon. *Geoscience Frontiers*, *13*(1), 101149. https://doi.org/10.1016/j.gsf.2021.101149

Bond, T. C., Doherty, S. J., Fahey, D. W., Forster, P. M., Berntsen, T., DeAngelo, B. J., et al. (2013). Bounding the role of black carbon in the climate system: A scientific assessment. *Journal of Geophysical Research: Atmospheres*, *118*(11), 5380–5552. https://doi.org/10.1002/jgrd.50171

Boucher, O., Servonnat, J., Albright, A. L., Aumont, O., Balkanski, Y., Bastrikov, V., et al. (2020). Presentation and Evaluation of the IPSL-CM6A-LR Climate Model. *Journal of Advances in Modeling Earth Systems*, *12*(7), e2019MS002010. https://doi.org/10.1029/2019MS002010

Browse, J., Carslaw, K. S., Arnold, S. R., Pringle, K., & Boucher, O. (2012). The scavenging processes controlling the seasonal cycle in Arctic sulphate and black carbon aerosol. *Atmospheric Chemistry and Physics*, *12*(15), 6775–6798. https://doi.org/10.5194/acp-12-6775-2012

https://doi.org/10.5194/egusphere-2026-2728
Preprint. Discussion started: 4 August 2026

Brugger, S. O., Schwikowski, M., Gobet, E., Schwörer, C., Rohr, C., Sigl, M., et al. (2021). Alpine Glacier Reveals Ecosystem Impacts of Europe's Prosperity and Peril Over the Last Millennium. *Geophysical Research Letters*, *48*(20), e2021GL095039. https://doi.org/10.1029/2021GL095039

Cahoon, D. R., Stocks, B. J., Levine, J. S., Cofer, W. R., & O'Neill, K. P. (1992). Seasonal distribution of African savanna fires. *Nature*, *359*(6398), 812–815. https://doi.org/10.1038/359812a0

Cape, J. N., Coyle, M., & Dumitrean, P. (2012). The atmospheric lifetime of black carbon. *Atmospheric Environment*, *59*, 256–263. https://doi.org/10.1016/j.atmosenv.2012.05.030

Carslaw, Lee, L. A., Reddington, C. L., Pringle, K. J., Rap, A., Forster, P. M., et al. (2013). Large contribution of natural aerosols to uncertainty in indirect forcing. *Nature*, *503*(7474), 67–71. https://doi.org/10.1038/nature12674

Carslaw, Gordon, H., Hamilton, D. S., Johnson, J. S., Regayre, L. A., Yoshioka, M., & Pringle, K. J. (2017). Aerosols in the Pre-industrial Atmosphere. *Current Climate Change Reports*, *3*(1), 1–15. https://doi.org/10.1007/s40641-017-0061-2

Chellman, N., McConnell, J. R., Arienzo, M., Pederson, G. T., Aarons, S. M., & Csank, A. (2017). Reassessment of the Upper Fremont Glacier Ice-Core Chronologies by Synchronizing of Ice-Core-Water Isotopes to a Nearby Tree-Ring Chronology. *Environmental Science & Technology*, *51*(8), 4230–4238. https://doi.org/10.1021/acs.est.6b06574

Chen, Y., Li, X., Xing, Y., Yan, S., Wu, D., Shi, T., et al. (2022). Historical Changes of Black Carbon in Snow and Its Radiative Forcing in CMIP6 Models. *Atmosphere*, *13*(11), 1774. https://doi.org/10.3390/atmos13111774

Chen, Y., Hall, J., van Wees, D., Andela, N., Hantson, S., Giglio, L., et al. (2023). Multi-decadal trends and variability in burned area from the fifth version of the Global Fire Emissions Database (GFED5). *Earth System Science Data*, *15*(11), 5227–5259. https://doi.org/10.5194/essd-15-5227-2023

Chen, Y., Xing, Y., Yan, S., Hou, Y., Li, X., Shi, T., et al. (2024). A Comprehensive Evaluation of Black Carbon in Snow and Its Radiative Forcing in CMIP5 and CMIP6 Models Based on Global Field Observations. *Journal of Geophysical Research: Atmospheres*, *129*(14), e2023JD040665. https://doi.org/10.1029/2023JD040665

Clifton, O. E., Bauer, S. E., Tsigaridis, K., Aleinov, I., Cowan, T. G., Faluvegi, G., & Kelley, M. (2024). Influence of More Mechanistic Representation of Particle Dry Deposition on 1850–2000 Changes in Global Aerosol Burdens and Radiative Forcing. *Journal of Advances in Modeling Earth Systems*, *16*(3), e2023MS003952. https://doi.org/10.1029/2023MS003952

Collins, W. J., Lamarque, J.-F., Schulz, M., Boucher, O., Eyring, V., Hegglin, M. I., et al. (2017). AerChemMIP: quantifying the effects of chemistry and aerosols in CMIP6. *Geoscientific Model Development*, *10*(2), 585–607. https://doi.org/10.5194/gmd-10-585-2017

Conway, H., Gades, A., & Raymond, C. F. (1996). Albedo of dirty snow during conditions of melt. *Water Resources Research*, *32*(6), 1713–1718. https://doi.org/10.1029/96WR00712

Cordell, R. L., Mazet, M., Dechoux, C., Hama, S. M. L., Staelens, J., Hofman, J., et al. (2016). Evaluation of biomass burning across North West Europe and its impact on air quality. *Atmospheric Environment*, *141*, 276–286. https://doi.org/10.1016/j.atmosenv.2016.06.065

Cozic, J., Verheggen, B., Mertes, S., Connolly, P., Bower, K., Petzold, A., et al. (2007). Scavenging of black carbon in mixed phase clouds at the high alpine site Jungfraujoch. *Atmospheric Chemistry and Physics*, *7*(7), 1797–1807. https://doi.org/10.5194/acp-7-1797-2007

Cozic, J., Mertes, S., Verheggen, B., Cziczo, D. J., Gallavardin, S. J., Walter, S., et al. (2008). Black carbon enrichment in atmospheric ice particle residuals observed in lower tropospheric mixed phase clouds. *Journal of Geophysical Research: Atmospheres*, *113*(D15). https://doi.org/10.1029/2007JD009266

Doherty, Warren, S. G., Grenfell, T. C., Clarke, A. D., & Brandt, R. E. (2010). Light-absorbing impurities in Arctic snow. *Atmospheric Chemistry and Physics*, *10*(23), 11647–11680. https://doi.org/10.5194/acp-10-11647-2010

Doherty, Grenfell, T. C., Forsström, S., Hegg, D. L., Brandt, R. E., & Warren, S. G. (2013). Observed vertical redistribution of black carbon and other insoluble light-absorbing particles in melting snow. *Journal of Geophysical Research: Atmospheres*, *118*(11), 5553–5569. https://doi.org/10.1002/jgrd.50235

Döscher, R., Acosta, M., Alessandri, A., Anthoni, P., Arsouze, T., Bergman, T., et al. (2022). The EC-Earth3 Earth system model for the Coupled Model Intercomparison Project 6. *Geoscientific Model Development*, *15*(7), 2973–3020. https://doi.org/10.5194/gmd-15-2973-2022

Durack, P. J., Naik, V., Nicholls, Z., O'Rourke, E., Turner, B., Buontempo, C., et al. (2025). Earth System Forcing for CMIP7 and Beyond. https://doi.org/10.1175/BAMS-D-25-0119.1

Eckhardt, S., Pisso, I., Evangeliou, N., Zwaaftink, C. G., Plach, A., McConnell, J. R., et al. (2023). Revised historical Northern Hemisphere black carbon emissions based on inverse modeling of ice core records. *Nature Communications*, *14*(1), 271. https://doi.org/10.1038/s41467-022-35660-0

Eichler, A., Schwikowski, M., Gäggeler, H. W., Furrer, V., Synal, H.-A., Beer, J., et al. (2000). Glaciochemical dating of an ice core from upper Grenzgletscher (4200 m a.s.l.). *Journal of Glaciology*, *46*(154), 507–515. https://doi.org/10.3189/172756500781833098

Elson, P., Andrade, E. S. de, Lucas, G., May, R., Hattersley, R., Campbell, E., et al. (2024, October 8). SciTools/cartopy: REL: v0.24.1 (Version v0.24.1). Zenodo. https://doi.org/10.5281/zenodo.13905945

Emerson, E. W., Hodshire, A. L., DeBolt, H. M., Bilsback, K. R., Pierce, J. R., McMeeking, G. R., & Farmer, D. K. (2020). Revisiting particle dry deposition and its role in radiative

https://doi.org/10.5194/egusphere-2026-2728
Preprint. Discussion started: 4 August 2026

effect estimates. *Proceedings of the National Academy of Sciences*, *117*(42), 26076–26082. https://doi.org/10.1073/pnas.2014761117

Eyring, V., Bony, S., Meehl, G. A., Senior, C. A., Stevens, B., Stouffer, R. J., & Taylor, K. E. (2016). Overview of the Coupled Model Intercomparison Project Phase 6 (CMIP6) experimental design and organization. *Geoscientific Model Development*, *9*(5), 1937–1958. https://doi.org/10.5194/gmd-9-1937-2016

Faïn, X., Szopa, S., Naïk, V., Martinerie, P., Etheridge, D. M., Rhodes, R. H., et al. (2025). Preindustrial-to-present-day changes in atmospheric carbon monoxide: agreement and gaps between ice archives and global model reconstructions. *Atmospheric Chemistry and Physics*, *25*(2), 1105–1119. https://doi.org/10.5194/acp-25-1105-2025

Fang, L., Jenk, T. M., and Schwikowski, M.: Radiocarbon dating of alpine ice cores, Past Glob. Chang. Mag., 31, 106–107, https://doi.org/10.22498/pages.31.2.106, 2023.

Farmer, D. K., Boedicker, E. K., & DeBolt, H. M. (2021). Dry Deposition of Atmospheric Aerosols: Approaches, Observations, and Mechanisms. *Annual Review of Physical Chemistry*, *72*(Volume 72, 2021), 375–397. https://doi.org/10.1146/annurev-physchem-090519-034936

Foley, J. A., DeFries, R., Asner, G. P., Barford, C., Bonan, G., Carpenter, S. R., et al. (2005). Global Consequences of Land Use. *Science*, *309*(5734), 570–574. https://doi.org/10.1126/science.1111772

Gabbi, J., Huss, M., Bauder, A., Cao, F., & Schwikowski, M. (2015). The impact of Saharan dust and black carbon on albedo and long-term mass balance of an Alpine glacier. *The Cryosphere*, *9*(4), 1385–1400. https://doi.org/10.5194/tc-9-1385-2015

Giglio, L., Boschetti, L., Roy, D. P., Humber, M. L., & Justice, C. O. (2018). The Collection 6 MODIS burned area mapping algorithm and product. *Remote Sensing of Environment*, *217*, 72–85. https://doi.org/10.1016/j.rse.2018.08.005

Ginot, P., Dumont, M., Lim, S., Patris, N., Taupin, J.-D., Wagnon, P., et al. (2014). A 10 year record of black carbon and dust from a Mera Peak ice core (Nepal): variability and potential impact on melting of Himalayan glaciers. *The Cryosphere*, *8*(4), 1479–1496. https://doi.org/10.5194/tc-8-1479-2014

Ginot, Patrick, Kull, C., Schwikowski, M., Schotterer, U., & Gäggeler, H. W. (2001). Effects of post-depositional processes on snow composition of a subtropical glacier (Cerro Tapado, Chilean Andes). *Journal of Geophysical Research: Atmospheres*, *106*(D23), 32375–32386. https://doi.org/10.1029/2000JD000071

Goldewijk, K. K. (2005). Three Centuries of Global Population Growth: A Spatial Referenced Population (Density) Database for 1700–2000. *Population and Environment*, *26*(4), 343–367. https://doi.org/10.1007/s11111-005-3346-7

Guo, Z., Li, W., Ciais, P., Sitch, S., van der Werf, G. R., Bowring, S. P. K., et al. (2025). Reconstructed global monthly burned area maps from 1901 to 2020. *Earth System Science Data Discussions*, 1–28. https://doi.org/10.5194/essd-2024-556

https://doi.org/10.5194/egusphere-2026-2728
Preprint. Discussion started: 4 August 2026

Hadley, O. L., & Kirchstetter, T. W. (2012). Black-carbon reduction of snow albedo. *Nature Climate Change*, *2*(6), 437–440. https://doi.org/10.1038/nclimate1433

Hamilton, Lee, L. A., Pringle, K. J., Reddington, C. L., Spracklen, D. V., & Carslaw, K. S. (2014). Occurrence of pristine aerosol environments on a polluted planet. *Proceedings of the National Academy of Sciences*, *111*(52), 18466–18471. https://doi.org/10.1073/pnas.1415440111

Hamilton, Hantson, S., Scott, C. E., Kaplan, J. O., Pringle, K. J., Nieradzik, L. P., et al. (2018). Reassessment of pre-industrial fire emissions strongly affects anthropogenic aerosol forcing. *Nature Communications*, *9*(1), 3182. https://doi.org/10.1038/s41467-018-05592-9

Hansen, J., & Nazarenko, L. (2004). Soot climate forcing via snow and ice albedos. *Proceedings of the National Academy of Sciences*, *101*(2), 423–428. https://doi.org/10.1073/pnas.2237157100

Harris, C. R., Millman, K. J., van der Walt, S. J., Gommers, R., Virtanen, P., Cournapeau, D., et al. (2020). Array programming with NumPy. *Nature*, *585*(7825), 357–362. https://doi.org/10.1038/s41586-020-2649-2

Herron, M. M., & Jr, C. C. L. (1980). Firn Densification: An Empirical Model. *Journal of Glaciology*, *25*(93), 373–385. https://doi.org/10.3189/S0022143000015239

Hoesly, R. M., Smith, S. J., Feng, L., Klimont, Z., Janssens-Maenhout, G., Pitkanen, T., et al. (2018). Historical (1750–2014) anthropogenic emissions of reactive gases and aerosols from the Community Emissions Data System (CEDS). *Geoscientific Model Development*, *11*(1), 369–408. https://doi.org/10.5194/gmd-11-369-2018

Hu, D., Alfarra, M. R., Szpek, K., Langridge, J. M., Cotterell, M. I., Belcher, C., et al. (2021). Physical and chemical properties of black carbon and organic matter from different combustion and photochemical sources using aerodynamic aerosol classification. *Atmospheric Chemistry and Physics*, *21*(21), 16161–16182. https://doi.org/10.5194/acp-21-16161-2021

Hunter, J. D. (2007). Matplotlib: A 2D Graphics Environment. *Computing in Science & Engineering*, *9*(3), 90–95. https://doi.org/10.1109/MCSE.2007.55

van den Hurk, B., Kim, H., Krinner, G., Seneviratne, S. I., Derksen, C., Oki, T., et al. (2016). LS3MIP (v1.0) contribution to CMIP6: the Land Surface, Snow and Soil moisture Model Intercomparison Project – aims, setup and expected outcome. *Geoscientific Model Development*, *9*(8), 2809–2832. https://doi.org/10.5194/gmd-9-2809-2016

IPCC. (2021). *Climate Change 2021: The Physical Science Basis. Contribution of Working Group I to the Sixth Assessment Report of the Intergovernmental Panel on Climate Change* (Vol. In Press). Cambridge, United Kingdom and New York, NY, USA: Cambridge University Press. https://doi.org/10.1017/9781009157896

Jacobson, M. Z. (2004). Climate response of fossil fuel and biofuel soot, accounting for soot's feedback to snow and sea ice albedo and emissivity. *Journal of Geophysical Research: Atmospheres*, *109*(D21). https://doi.org/10.1029/2004JD004945

https://doi.org/10.5194/egusphere-2026-2728
Preprint. Discussion started: 4 August 2026

Jenk, T. M., Szidat, S., Schwikowski, M., Gäggeler, H. W., Brütsch, S., Wacker, L., et al. (2006). Radiocarbon analysis in an Alpine ice core: record of anthropogenic and biogenic contributions to carbonaceous aerosols in the past (1650–1940). *Atmospheric Chemistry and Physics*, *6*(12), 5381–5390. https://doi.org/10.5194/acp-6-5381-2006

Jethva, H., Torres, O., Field, R. D., Lyapustin, A., Gautam, R., & Kayetha, V. (2019). Connecting Crop Productivity, Residue Fires, and Air Quality over Northern India. *Scientific Reports*, *9*(1), 16594. https://doi.org/10.1038/s41598-019-52799-x

Jiménez-Moreno, G., Fawcett, P. J., & Scott Anderson, R. (2008). Millennial- and centennial-scale vegetation and climate changes during the late Pleistocene and Holocene from northern New Mexico (USA). *Quaternary Science Reviews*, *27*(13), 1442–1452. https://doi.org/10.1016/j.quascirev.2008.04.004

Jones, M. W., Abatzoglou, J. T., Veraverbeke, S., Andela, N., Lasslop, G., Forkel, M., et al. (2022). Global and Regional Trends and Drivers of Fire Under Climate Change. *Reviews of Geophysics*, *60*(3), e2020RG000726. https://doi.org/10.1029/2020RG000726

Kaspari, S. D., Pittenger, D., Jenk, T. M., Morgenstern, U., Schwikowski, M., Buenning, N., and Stott, L.: Twentieth Century Black Carbon and Dust Deposition on South Cascade Glacier, Washington State, USA, as Reconstructed From a 158-m-Long Ice Core, J. Geophys. Res. Atmos., 125, 1–19, https://doi.org/10.1029/2019JD031126, 2020.

Kang, S., Zhang, Y., Qian, Y., & Wang, H. (2020). A review of black carbon in snow and ice and its impact on the cryosphere. *Earth-Science Reviews*, *210*, 103346. https://doi.org/10.1016/j.earscirev.2020.103346

Kaplan, J. O., Krumhardt, K. M., & Zimmermann, N. (2009). The prehistoric and preindustrial deforestation of Europe. *Quaternary Science Reviews*, *28*(27), 3016–3034. https://doi.org/10.1016/j.quascirev.2009.09.028

Kaplan, J. O., Krumhardt, K. M., Gaillard, M.-J., Sugita, S., Trondman, A.-K., Fyfe, R., et al. (2017). Constraining the Deforestation History of Europe: Evaluation of Historical Land Use Scenarios with Pollen-Based Land Cover Reconstructions. *Land*, *6*(4), 91. https://doi.org/10.3390/land6040091

Kawamiya, M., Hajima, T., Tachiiri, K., Watanabe, S., & Yokohata, T. (2020). Two decades of Earth system modeling with an emphasis on Model for Interdisciplinary Research on Climate (MIROC). *Progress in Earth and Planetary Science*, *7*(1), 64. https://doi.org/10.1186/s40645-020-00369-5

Kay, J. E., Deser, C., Phillips, A., Mai, A., Hannay, C., Strand, G., et al. (2015). The Community Earth System Model (CESM) Large Ensemble Project: A Community Resource for Studying Climate Change in the Presence of Internal Climate Variability. https://doi.org/10.1175/BAMS-D-13-00255.1

Kelley, D. I., Bistinas, I., Whitley, R., Burton, C., Marthews, T. R., & Dong, N. (2019). How contemporary bioclimatic and human controls change global fire regimes. *Nature Climate Change*, *9*(9), 690–696. https://doi.org/10.1038/s41558-019-0540-7

https://doi.org/10.5194/egusphere-2026-2728
Preprint. Discussion started: 4 August 2026

Kharol, S. K., Badarinath, K. V. S., Sharma, A. R., Mahalakshmi, D. V., Singh, D., & Prasad, V. K. (2012). Black carbon aerosol variations over Patiala city, Punjab, India—A study during agriculture crop residue burning period using ground measurements and satellite data. *Journal of Atmospheric and Solar-Terrestrial Physics*, *84–85*, 45–51. https://doi.org/10.1016/j.jastp.2012.05.013

Knorr, W., Kaminski, T., Arneth, A., & Weber, U. (2014). Impact of human population density on fire frequency at the global scale. *Biogeosciences*, *11*(4), 1085–1102. https://doi.org/10.5194/bg-11-1085-2014

Koch, D., & Del Genio, A. D. (2010). Black carbon semi-direct effects on cloud cover: review and synthesis. *Atmospheric Chemistry and Physics*, *10*(16), 7685–7696. https://doi.org/10.5194/acp-10-7685-2010

Koopmans, & Koppejan. (1997). Agricultural and Forest Residues—Generation, Utilization and Availability. Regional Wood Energy Development Programs, Asia. *Scientific Research Publishing*. Retrieved from https://www.scirp.org/reference/referencespapers?referenceid=3340306

Lee, Y. H., Lamarque, J.-F., Flanner, M. G., Jiao, C., Shindell, D. T., Berntsen, T., et al. (2013). Evaluation of preindustrial to present-day black carbon and its albedo forcing from Atmospheric Chemistry and Climate Model Intercomparison Project (ACCMIP). *Atmospheric Chemistry and Physics*, *13*(5), 2607–2634. https://doi.org/10.5194/acp-13-2607-2013

Legrand, M., & De Angelis, M. (1996). Light carboxylic acids in Greenland ice: A record of past forest fires and vegetation emissions from the boreal zone. *Journal of Geophysical Research: Atmospheres*, *101*(D2), 4129–4145. https://doi.org/10.1029/95JD03296

Li, F., Val Martin, M., Hantson, S., Andreae, M. O., Arneth, A., Lasslop, G., Yue, C., Bachelet, D., Forrest, M., Kaiser, J. W., Kluzek, E., Liu, X., Melton, J. R., Ward, D. S., Darmenov, A., Hickler, T., Ichoku, C., Magi, B. I., Sitch, S., van der Werf, G. R., and Wiedinmyer, C.: Historical (1700-2012) Global Multi-model Estimates of the Fire Emissions from the Fire Modeling Intercomparison Project (FireMIP), Atmos. Chem. Phys. Discuss., 1–57, https://doi.org/10.5194/acp-2019-37, 2019.

Li, Y., & Flanner, M. G. (2018). Investigating the impact of aerosol deposition on snowmelt over the Greenland Ice Sheet using a large-ensemble kernel. *Atmospheric Chemistry and Physics*, *18*(21), 16005–16018. https://doi.org/10.5194/acp-18-16005-2018

Liefeld, J. (2025, June 23). InterpolateScalingPy (Version 1.0). Retrieved from https://doi.org/10.5281/zenodo.15733193

Liou, K. N., Takano, Y., & Yang, P. (2011). Light absorption and scattering by aggregates: Application to black carbon and snow grains. *Journal of Quantitative Spectroscopy and Radiative Transfer*, *112*(10), 1581–1594. https://doi.org/10.1016/j.jqsrt.2011.03.007

Liu, He, C., Schwarz, J. P., & Wang, X. (2020). Lifecycle of light-absorbing carbonaceous aerosols in the atmosphere. *Npj Climate and Atmospheric Science*, *3*(1), 1–18. https://doi.org/10.1038/s41612-020-00145-8

https://doi.org/10.5194/egusphere-2026-2728
Preprint. Discussion started: 4 August 2026

Liu, Kaplan, J. O., Mickley, L. J., Li, Y., Chellman, N. J., Arienzo, M. M., et al. (2021). Improved estimates of preindustrial biomass burning reduce the magnitude of aerosol climate forcing in the Southern Hemisphere. *Science Advances*, *7*(22), eabc1379. https://doi.org/10.1126/sciadv.abc1379

Liu, Schuster, G. L., Moosmüller, H., Stamnes, S., Cairns, B., & Chowdhary, J. (2022). Optical properties of morphologically complex black carbon aerosols: Effects of coatings. *Journal of Quantitative Spectroscopy and Radiative Transfer*, *281*, 108080. https://doi.org/10.1016/j.jqsrt.2022.108080

Liu, X., Zhang, X., Huang, Y., Chen, K., Wang, L., Ma, J., et al. (2021). The Direct Radiative Forcing Impact of Agriculture-Emitted Black Carbon Associated With India's Green Revolution. *Earth's Future*, *9*(6), e2021EF001975. https://doi.org/10.1029/2021EF001975

Ma, X., & Wang, A. (2024). Evaluation and Uncertainty Analysis of the Land Surface Hydrology in LS3MIP Models Over China. *Earth and Space Science*, *11*(7), e2023EA003391. https://doi.org/10.1029/2023EA003391

Mahowald, N. M., Li, L., Albani, S., Hamilton, D. S., & Kok, J. F. (2024). Opinion: The importance of historical and paleoclimate aerosol radiative effects. *Atmospheric Chemistry and Physics*, *24*(1), 533–551. https://doi.org/10.5194/acp-24-533-2024

van Marle, M. J. E., Kloster, S., Magi, B. I., Marlon, J. R., Daniau, A.-L., Field, R. D., et al. (2017). Historic global biomass burning emissions for CMIP6 (BB4CMIP) based on merging satellite observations with proxies and fire models (1750–2015). *Geoscientific Model Development*, *10*(9), 3329–3357. https://doi.org/10.5194/gmd-10-3329-2017

Marlon, J. R., Bartlein, P. J., Carcaillet, C., Gavin, D. G., Harrison, S. P., Higuera, P. E., et al. (2008). Climate and human influences on global biomass burning over the past two millennia. *Nature Geoscience*, *1*(10), 697–702. https://doi.org/10.1038/ngeo313

Maselli, O. J., Fritzsche ,Diedrich, Layman ,Lawrence, McConnell ,Joseph R., & and Meyer, H. (2013). Comparison of water isotope-ratio determinations using two cavity ring-down instruments and classical mass spectrometry in continuous ice-core analysis. *Isotopes in Environmental and Health Studies*, *49*(3), 387–398. https://doi.org/10.1080/10256016.2013.781598

McConnell, J. R. (2010). New Directions: Historical black carbon and other ice core aerosol records in the Arctic for GCM evaluation. *Atmospheric Environment*, *44*(21), 2665–2666. https://doi.org/10.1016/j.atmosenv.2010.04.004

McConnell, J. R., Edwards, R., Kok, G. L., Flanner, M. G., Zender, C. S., Saltzman, E. S., et al. (2007). 20th-Century Industrial Black Carbon Emissions Altered Arctic Climate Forcing. *Science*, *317*(5843), 1381–1384. https://doi.org/10.1126/science.1144856

Ming, J., Cachier, H., Xiao, C., Qin, D., Kang, S., Hou, S., & Xu, J. (2008). Black carbon record based on a shallow Himalayan ice core and its climatic implications. *Atmospheric Chemistry and Physics*, *8*(5), 1343–1352. https://doi.org/10.5194/acp-8-1343-2008

https://doi.org/10.5194/egusphere-2026-2728
Preprint. Discussion started: 4 August 2026

Mollicone, D., Eva, H. D., & Achard, F. (2006). Human role in Russian wild fires. *Nature*, *440*(7083), 436–437. https://doi.org/10.1038/440436a

Moseid, K. O., Schulz, M., Eichler, A., Schwikowski, M., McConnell, J. R., Olivié, D., et al. (2022). Using Ice Cores to Evaluate CMIP6 Aerosol Concentrations Over the Historical Era. *Journal of Geophysical Research: Atmospheres*, *127*(18). https://doi.org/10.1029/2021JD036105

Nikonovas, T., Spessa, A., Doerr, S. H., Clay, G. D., & Mezbahuddin, S. (2020). Near-complete loss of fire-resistant primary tropical forest cover in Sumatra and Kalimantan. *Communications Earth & Environment*, *1*(1), 65. https://doi.org/10.1038/s43247-020-00069-4

Osmont, D., Wendl, I. A., Schmidely, L., Sigl, M., Vega, C. P., Isaksson, E., & Schwikowski, M. (2018). An 800-year high-resolution black carbon ice core record from Lomonosovfonna, Svalbard. *Atmospheric Chemistry and Physics*, *18*(17), 12777–12795. https://doi.org/10.5194/acp-18-12777-2018

Oyabu, I., Kawamura, K., Uchida, T., Fujita, S., Kitamura, K., Hirabayashi, M., et al. (2021). Fractionation of O_2/N_2 and Ar/N_2 in the Antarctic ice sheet during bubble formation and bubble–clathrate hydrate transition from precise gas measurements of the Dome Fuji ice core. *The Cryosphere*, *15*(12), 5529–5555. https://doi.org/10.5194/tc-15-5529-2021

Park, Cao, Kittelson, & McMurry. (2003). Relationship between Particle Mass and Mobility for Diesel Exhaust Particles. *Environmental Science & Technology*. https://doi.org/10.1021/es025960v

Pausas, J. G., & Keeley, J. E. (2014). Abrupt Climate-Independent Fire Regime Changes. *Ecosystems*, *17*(6), 1109–1120. https://doi.org/10.1007/s10021-014-9773-5

Pechony, O., & Shindell, D. T. (2010). Driving forces of global wildfires over the past millennium and the forthcoming century. *Proceedings of the National Academy of Sciences*, *107*(45), 19167–19170. https://doi.org/10.1073/pnas.1003669107

Petroff, A., & Zhang, L. (2010). Development and validation of a size-resolved particle dry deposition scheme for application in aerosol transport models. *Geoscientific Model Development*, *3*(2), 753–769. https://doi.org/10.5194/gmd-3-753-2010

Pinglot, J. F., Vaikmäe, R. A., Kamiyama, K., Igarashi, M., Fritzsche, D., Wilhelms, F., Koerner, R., Henderson, L., Isaksson, E., Winther, J. G., Van De Wal, R. S. W., Fournier, M., Bouisset, P., and Meijer, H. A. J.: Ice cores from Arctic sub-polar glaciers: Chronology and post-depositional processes deduced from radioactivity measurements, J. Glaciol., 49, 149–158, https://doi.org/10.3189/172756503781830944, 2003.

Pleim, J. E., Ran, L., Saylor, R. D., Willison, J., & Binkowski, F. S. (2022). A New Aerosol Dry Deposition Model for Air Quality and Climate Modeling. *Journal of Advances in Modeling Earth Systems*, *14*(11), e2022MS003050. https://doi.org/10.1029/2022MS003050

Rabin, S. S., Melton, J. R., Lasslop, G., Bachelet, D., Forrest, M., Hantson, S., et al. (2017). The Fire Modeling Intercomparison Project (FireMIP), phase 1: experimental and analytical

https://doi.org/10.5194/egusphere-2026-2728
Preprint. Discussion started: 4 August 2026

protocols with detailed model descriptions. *Geoscientific Model Development*, *10*(3), 1175–1197. https://doi.org/10.5194/gmd-10-1175-2017

Reisinger, P., Wonaschütz, A., Hitzenberger, R., Petzold, A., Bauer, H., Jankowski, N., et al. (2008). Intercomparison of Measurement Techniques for Black or Elemental Carbon Under Urban Background Conditions in Wintertime: Influence of Biomass Combustion. *Environmental Science & Technology*, *42*(3), 884–889. https://doi.org/10.1021/es0715041

Ren, Y., Oxford, C., Zhang, D., Liu, X., Zhu, H., Dillner, A., et al. (2025, February 17). Black Carbon Emissions Generally Underestimated in the Global South as Revealed by Globally Distributed Measurements. Research Square. https://doi.org/10.21203/rs.3.rs-6024974/v1

Robock, A., & Graf, H.-F. (1994). Effects of pre-industrial human activities on climate. *Chemosphere*, *29*(5), 1087–1097. https://doi.org/10.1016/0045-6535(94)90169-4

Röckmann, T., Gómez Álvarez, C. X., Walter, S., van der Veen, C., Wollny, A. G., Gunthe, S. S., et al. (2010). Isotopic composition of H2 from wood burning: Dependency on combustion efficiency, moisture content, and δD of local precipitation. *Journal of Geophysical Research: Atmospheres*, *115*(D17). https://doi.org/10.1029/2009JD013188

Roehrig, R., Beau, I., Saint-Martin, D., Alias, A., Decharme, B., Guérémy, J.-F., et al. (2020). The CNRM Global Atmosphere Model ARPEGE-Climat 6.3: Description and Evaluation. *Journal of Advances in Modeling Earth Systems*, *12*(7), e2020MS002075. https://doi.org/10.1029/2020MS002075

Rowlinson, M. J., Rap, A., Hamilton, D. S., Pope, R. J., Hantson, S., Arnold, S. R., et al. (2020). Tropospheric ozone radiative forcing uncertainty due to pre-industrial fire and biogenic emissions. *Atmospheric Chemistry and Physics*, *20*(18), 10937–10951. https://doi.org/10.5194/acp-20-10937-2020

Rudel, T. K., Defries, R., Asner, G. P., & Laurance, W. F. (2009). Changing Drivers of Deforestation and New Opportunities for Conservation. *Conservation Biology*, *23*(6), 1396–1405. https://doi.org/10.1111/j.1523-1739.2009.01332.x

Ryan, K. C., Knapp, E. E., & Varner, J. M. (2013). Prescribed fire in North American forests and woodlands: history, current practice, and challenges. *Frontiers in Ecology and the Environment*, *11*(s1), e15–e24. https://doi.org/10.1890/120329

Sahu, S. K., Beig, G., & Sharma, C. (2008). Decadal growth of black carbon emissions in India. *Geophysical Research Letters*, *35*(2). https://doi.org/10.1029/2007GL032333

Saylor, R. D., Baker ,Barry D., Lee ,Pius, Tong ,Daniel, Pan ,Li, & and Hicks, B. B. (2019). The particle dry deposition component of total deposition from air quality models: right, wrong or uncertain? *Tellus B: Chemical and Physical Meteorology*, *71*(1), 1550324. https://doi.org/10.1080/16000889.2018.1550324

Schmitt, C. G., Riggs, B. L., Horodyskyj, U. N., Khan, A. L., Ewing, H. A., All, J. D., & Sanchez Rodriguez, W. (2019). The measurement and impact of light absorbing particles

https://doi.org/10.5194/egusphere-2026-2728
Preprint. Discussion started: 4 August 2026

on snow surfaces. *The Cryosphere Discussions*, 1–16. https://doi.org/10.5194/tc-2019-162

Schulzweida, U. (2023). CDO User Guide. https://doi.org/10.5281/zenodo.10020800

Schurer, A. P., Mann, M. E., Hawkins, E., Tett, S. F. B., & Hegerl, G. C. (2017). Importance of the pre-industrial baseline for likelihood of exceeding Paris goals. *Nature Climate Change*, *7*(8), 563–567. https://doi.org/10.1038/nclimate3345

Schwarz, J. P., Gao, R. S., Perring, A. E., Spackman, J. R., & Fahey, D. W. (2013). Black carbon aerosol size in snow. *Scientific Reports*, *3*(1), 1356. https://doi.org/10.1038/srep01356

Seinfeld, J., & Pandis, S. (2016). *Atmospheric Chemistry and Physics: From Air Pollution to Climate Change, 3rd Edition | Wiley* (3rd ed.). Wiley. Retrieved from https://www.wiley.com/en-us/Atmospheric+Chemistry+and+Physics%3A+From+Air+Pollution+to+Climate+Change%2C+3rd+Edition-p-9781118947401

Shen, W., Wang, M., Liu, Y., Dong, X., Zhao, D., Yue, M., et al. (2023). Evaluating BC Aging Processes in the Community Atmosphere Model Version 6 (CAM6). *Journal of Geophysical Research: Atmospheres*, *128*(3), e2022JD037427. https://doi.org/10.1029/2022JD037427

Sigl, M., Fudge, T. J., Winstrup, M., Cole-Dai, J., Ferris, D., McConnell, J. R., Taylor, K. C., Welten, K. C., Woodruff, T. E., Adolphi, F., Bisiaux, M., Brook, E. J., Buizert, C., Caffee, M. W., Dunbar, N. W., Edwards, R., Geng, L., Iverson, N., Koffman, B., Layman, L., Maselli, O. J., McGwire, K., Muscheler, R., Nishiizumi, K., Pasteris, D. R., Rhodes, R. H., and Sowers, T. A.: The WAIS Divide deep ice core WD2014 chronology - Part 2: Annual-layer counting (0-31 ka BP), Clim. Past, 12, 769–786, https://doi.org/10.5194/cp-12-769-2016, 2016.Simpkins, G. (2018). Aerosol–cloud interactions. *Nature Climate Change*, *8*(6), 457–457. https://doi.org/10.1038/s41558-018-0195-9

Skiles, S. M., Flanner, M., Cook, J. M., Dumont, M., and Painter, T. H.: Radiative forcing by light-absorbing particles in snow, Nat. Clim. Chang., 8, 964–971, https://doi.org/10.1038/s41558-018-0296-5, 2018.

Staal, A., Tuinenburg, O. A., Bosmans, J. H. C., Holmgren, M., van Nes, E. H., Scheffer, M., et al. (2018). Forest-rainfall cascades buffer against drought across the Amazon. *Nature Climate Change*, *8*(6), 539–543. https://doi.org/10.1038/s41558-018-0177-y

Stohl, A. (2006). Characteristics of atmospheric transport into the Arctic troposphere. *Journal of Geophysical Research: Atmospheres*, *111*(D11). https://doi.org/10.1029/2005JD006888

Stohl, A., & Sodemann, H. (2010). Characteristics of atmospheric transport into the Antarctic troposphere. *Journal of Geophysical Research: Atmospheres*, *115*(D2). https://doi.org/10.1029/2009JD012536

Stohl, A., Berg, T., Burkhart, J. F., Fjǽraa, A. M., Forster, C., Herber, A., et al. (2007). Arctic smoke – record high air pollution levels in the European Arctic due to agricultural fires in

https://doi.org/10.5194/egusphere-2026-2728
Preprint. Discussion started: 4 August 2026

Eastern Europe in spring 2006. *Atmospheric Chemistry and Physics*, *7*(2), 511–534. https://doi.org/10.5194/acp-7-511-2007

Streets, D. G., Yarber, K. F., Woo, J.-H., & Carmichael, G. R. (2003). Biomass burning in Asia: Annual and seasonal estimates and atmospheric emissions. *Global Biogeochemical Cycles*, *17*(4). https://doi.org/10.1029/2003GB002040

Svensson, A., Dahl-Jensen, D., Steffensen, J. P., Blunier, T., Rasmussen, S. O., Vinther, B. M., et al. (2020). Bipolar volcanic synchronization of abrupt climate change in Greenland and Antarctic ice cores during the last glacial period. *Climate of the Past*, *16*(4), 1565–1580. https://doi.org/10.5194/cp-16-1565-2020

Swart, N. C., Cole, J. N. S., Kharin, V. V., Lazare, M., Scinocca, J. F., Gillett, N. P., et al. (2019). The Canadian Earth System Model version 5 (CanESM5.0.3). *Geoscientific Model Development*, *12*(11), 4823–4873. https://doi.org/10.5194/gmd-12-4823-2019

Targino, A. C., Krecl, P., Johansson, C., Swietlicki, E., Massling, A., Coraiola, G. C., & Lihavainen, H. (2013). Deterioration of air quality across Sweden due to transboundary agricultural burning emissions. *Boreal Environment Research*, *18*(1), 19–36.

Thevenon, F., Anselmetti, F. S., Bernasconi, S. M., & Schwikowski, M. (2009). Mineral dust and elemental black carbon records from an Alpine ice core (Colle Gnifetti glacier) over the last millennium. *Journal of Geophysical Research: Atmospheres*, *114*(D17). https://doi.org/10.1029/2008JD011490

Venkataraman, C., Habib, G., Kadamba, D., Shrivastava, M., Leon, J.-F., Crouzille, B., et al. (2006). Emissions from open biomass burning in India: Integrating the inventory approach with high-resolution Moderate Resolution Imaging Spectroradiometer (MODIS) active-fire and land cover data. *Global Biogeochemical Cycles*, *20*(2). https://doi.org/10.1029/2005GB002547

Vignati, E., Karl, M., Krol, M., Wilson, J., Stier, P., & Cavalli, F. (2010a). Sources of uncertainties in modelling black carbon at the global scale. *Atmospheric Chemistry and Physics*, *10*(6), 2595–2611. https://doi.org/10.5194/acp-10-2595-2010

Vignati, E., Karl, M., Krol, M., Wilson, J., Stier, P., & Cavalli, F. (2010b). Sources of uncertainties in modelling black carbon at the global scale. *Atmospheric Chemistry and Physics*, *10*(6), 2595–2611. https://doi.org/10.5194/acp-10-2595-2010

Virtanen, P., Gommers, R., Oliphant, T. E., Haberland, M., Reddy, T., Cournapeau, D., et al. (2020). SciPy 1.0: fundamental algorithms for scientific computing in Python. *Nature Methods*, *17*(3), 261–272. https://doi.org/10.1038/s41592-019-0686-2

Wan, J. S., Hamilton, D. S., & Mahowald, N. M. (2021). Importance of Uncertainties in the Spatial Distribution of Preindustrial Wildfires for Estimating Aerosol Radiative Forcing. *Geophysical Research Letters*, *48*(6), e2020GL089758. https://doi.org/10.1029/2020GL089758

Wang, M., Wang, H., Xu, B., Li, Z., Zhao, H., Li, J., et al. (2025). Radiocarbon Fingerprinting Black Carbon Source History in the Himalayas. *Geophysical Research Letters*, *52*(4), e2024GL113764. https://doi.org/10.1029/2024GL113764

https://doi.org/10.5194/egusphere-2026-2728
Preprint. Discussion started: 4 August 2026

Ward, D. S., Kloster, S., Mahowald, N. M., Rogers, B. M., Randerson, J. T., & Hess, P. G. (2012). The changing radiative forcing of fires: global model estimates for past, present and future. *Atmospheric Chemistry and Physics*, *12*(22), 10857–10886. https://doi.org/10.5194/acp-12-10857-2012

Ward, J. L., Flanner, M. G., Bergin, M., Dibb, J. E., Polashenski, C. M., Soja, A. J., & Thomas, J. L. (2018). Modeled Response of Greenland Snowmelt to the Presence of Biomass Burning-Based Absorbing Aerosols in the Atmosphere and Snow. *Journal of Geophysical Research: Atmospheres*, *123*(11), 6122–6141. https://doi.org/10.1029/2017JD027878

van der Werf, G. R., Randerson, J. T., Giglio, L., van Leeuwen, T. T., Chen, Y., Rogers, B. M., et al. (2017). Global fire emissions estimates during 1997–2016. *Earth System Science Data*, *9*(2), 697–720. https://doi.org/10.5194/essd-9-697-2017

Whitehair, L., Fulé, P. Z., Meador, A. S., Azpeleta Tarancón, A., & Kim, Y. (2018). Fire regime on a cultural landscape: Navajo Nation. *Ecology and Evolution*, *8*(19), 9848–9858. https://doi.org/10.1002/ece3.4470

Whitlow, S., Mayewski, P. A., & Dibb, J. E. (1992). A comparison of major chemical species seasonal concentration and accumulation at the South Pole and summit, Greenland. *Atmospheric Environment. Part A. General Topics*, *26*(11), 2045–2054. https://doi.org/10.1016/0960-1686(92)90089-4

Whitlow, S., Mayewski, P., Dibb, J., Holdsworth, G., & Twickler, M. (1994). An ice-core-based record of biomass burning in the Arctic and Subarctic, 1750–1980. *Tellus B*, *46*(3), 234–242. https://doi.org/10.1034/j.1600-0889.1994.t01-2-00006.x

Wolff, E. W., Chappellaz, J., Blunier, T., Rasmussen, S. O., & Svensson, A. (2010). Millennial-scale variability during the last glacial: The ice core record. *Quaternary Science Reviews*, *29*(21–22), 2828–2838. https://doi.org/10.1016/j.quascirev.2009.10.013

Xu, B., Cao, J., Hansen, J., Yao, T., Joswia, D. R., Wang, N., et al. (2009). Black soot and the survival of Tibetan glaciers. *Proceedings of the National Academy of Sciences*, *106*(52), 22114–22118. https://doi.org/10.1073/pnas.0910444106

Xu, B., Cao, J., Joswiak, D. R., Liu, X., Zhao, H., & He, J. (2012). Post-depositional enrichment of black soot in snow-pack and accelerated melting of Tibetan glaciers. *Environmental Research Letters*, *7*(1), 014022. https://doi.org/10.1088/1748-9326/7/1/014022

Yang, S., Xu, B., Cao, J., Zender, C. S., & Wang, M. (2015). Climate effect of black carbon aerosol in a Tibetan Plateau glacier. *Atmospheric Environment*, *111*, 71–78. https://doi.org/10.1016/j.atmosenv.2015.03.016

Yukimoto, S., Kawai, H., Koshiro, T., Oshima, N., Yoshida, K., Urakawa, S., et al. (2019). The Meteorological Research Institute Earth System Model Version 2.0, MRI-ESM2.0: Description and Basic Evaluation of the Physical Component. *Journal of the Meteorological Society of Japan. Ser. II*, *97*(5), 931–965. https://doi.org/10.2151/jmsj.2019-051

https://doi.org/10.5194/egusphere-2026-2728
Preprint. Discussion started: 4 August 2026

Zender, C. S. (2008). Analysis of self-describing gridded geoscience data with netCDF Operators (NCO). *Environmental Modelling & Software*, *23*(10), 1338–1342. https://doi.org/10.1016/j.envsoft.2008.03.004

Zhang, Gong, S., Padro, J., & Barrie, L. (2001). A size-segregated particle dry deposition scheme for an atmospheric aerosol module. *Atmospheric Environment*, *35*(3), 549–560. https://doi.org/10.1016/S1352-2310(00)00326-5

Zhang, Brook, J. R., & Vet, R. (2003). A revised parameterization for gaseous dry deposition in air-quality models. *Atmospheric Chemistry and Physics*, *3*(6), 2067–2082. https://doi.org/10.5194/acp-3-2067-2003

Zhang, Khalizov, A. F., Pagels, J., Zhang, D., Xue, H., & McMurry, P. H. (2008). Variability in morphology, hygroscopicity, and optical properties of soot aerosols during atmospheric processing. *Proceedings of the National Academy of Sciences*, *105*(30), 10291–10296. https://doi.org/10.1073/pnas.0804860105

Zhang, Wooster, M. J., Green, D. C., & Main, B. (2015). New field-based agricultural biomass burning trace gas, PM2.5, and black carbon emission ratios and factors measured *in situ* at crop residue fires in Eastern China. *Atmospheric Environment*, *121*, 22–34. https://doi.org/10.1016/j.atmosenv.2015.05.010

Zhang, Zhang, F., Zhang, G., & Yan, W. (2022). Why Do CMIP6 Models Fail to Simulate Snow Depth in Terms of Temporal Change and High Mountain Snow of China Skillfully? *Geophysical Research Letters*, *49*(15), e2022GL098888. https://doi.org/10.1029/2022GL098888

Zhang, Chellman, N. J., Kaplan, J. O., Mickley, L. J., Ito, T., Wang, X., et al. (2024). Improved biomass burning emissions from 1750 to 2010 using ice core records and inverse modeling. *Nature Communications*, *15*(1), 3651. https://doi.org/10.1038/s41467-024-47864-7

Zuo, J., & Qian, C. (2022). Evaluation of historical and future precipitation changes in CMIP6 over the Tarim River Basin. *Theoretical and Applied Climatology*, *150*(3), 1659–1675. https://doi.org/10.1007/s00704-022-04260-9